CHARACTERIZATION OF THE +SSTR AND ΔSSTR SPLICE VARIANTS OF THE $Ca_V2.1$ P/Q-TYPE VOLTAGE-GATED CALCIUM CHANNEL

by

Zeina Waheed

B.Sc. (Hons), The University of British Columbia, 2011

A THESIS SUBMITTED IN PARTIAL FULFILLMENT OF

THE REQUIREMENTS FOR THE DEGREE OF

MASTER OF SCIENCE

in

THE FACULTY OF GRADUATE AND POSTDOCTORAL STUDIES

(Neuroscience)

THE UNIVERSITY OF BRITISH COLUMBIA

(Vancouver)

October 2015

Abstract

$Ca_v2.1$ P/Q-type voltage-gated calcium channels are essential for neurotransmission in many regions of the mammalian central nervous system (CNS). Alternative splicing generates functional diversity between $Ca_v2.1$ splice isoforms and is thought to be a mechanism by which fine-tuning and complexity of $Ca_v2.1$-mediated activities occur. The $Ca_v2.1$ +SSTR splice variant, located in the S3-S4 linker of domain III, has been identified in rodent brain although its effects on the biophysical and pharmacological properties of $Ca_v2.1$ have not been previously studied. Here, by performing splice variant-specific quantitative real-time PCR on selected regions of the rat CNS I demonstrate that +SSTR variant channels are differentially expressed spatially with predominant expression in the brainstem, reticular thalamus and spinal cord. Using whole-cell patch-clamp electrophysiology performed on transfected HEK 293 cells I have shown that compared to ΔSSTR channels, +SSTR variants exhibit faster activation kinetics and a hyperpolarizing shift in the voltage-dependence of activation and inactivation. Additionally, the +SSTR and ΔSSTR variants respond differently to increasing durations of action potential waveforms (APWs) with the charge transference through +SSTR channels being significantly less sensitive to APW broadening than ΔSSTR channels. Together, these data suggest that the unique biophysical properties of the $Ca_v2.1$ splice variants contribute to distinct roles in CNS synaptic physiology by relaying different types of action potential-encoding synaptic information. Lastly, I examined whether the +SSTR variant affected the sensitivity of $Ca_v2.1$ to the gating modifier peptide toxin ω-Agatoxin-IVA. Using whole-cell patch-clamp electrophysiology I found that the effects of ω-Agatoxin-IVA on current block did not significantly differ between the +SSTR and ΔSSTR splice variants suggesting that SSTR insertion does not affect the binding of ω-Agatoxin-IVA to $Ca_v2.1$ channels. The differential

expression of $Ca_v2.1$ splice variants and their unique channel properties provides insight into the mechanisms by which complexity of P/Q-type calcium channel-mediated signaling contributes to CNS physiology.

Preface

The design of this research project was a joint effort between myself and Drs. Terry Snutch, Esperanza Garcia and John Tyson.

Dr. Stuart Cain performed the dissections of CNS tissues used for the qPCR experiments presented in Chapter 2 following UBC Animal Care Committee protocols (Animal Care Certificate # A12-0100) and according to the standards of the Canadian Council on Animal Care in Science.

I performed all experiments and analysis of the data. I also wrote this thesis including generating all figures and tables.

Table of Contents

List of Tables

List of Figures

List of Abbreviations

ANOVA	Analysis of variance
ATP	Adenosine triphosphate
Ba^{2+}	barium ion
BSA	Bovine Serum Albumin
Ca^{2+}	calcium ion
Ca_v	voltage-gated calcium channel
cDNA	complementary DNA
CDF	calcium-dependent facilitation
CDI	calcium-dependent inactivation
CNS	Central Nervous System
CO_2	Carbon dioxide
C_q	Quantification cycle
DNA	Deoxyribonucleic acid
EA2	Episodic ataxia type 2
eGFP	enhanced Green Fluorescent Protein
EGTA	Ethylene Glycol-bis(2-aminoethylether)-*N,N,N',N'*-Tetraacetic Acid
FHM1	Familial hemiplegic migraine type 1
GAPDH	Glyceraldehyde 3-phosphate dehydrogenase
HEK	Human Embryonic Kidney
HEPES	4-(2-Hydroxyethyl)piperazine-1-ethanesulfonic acid
HVA	High voltage-activated
IV	Current-Voltage

LVA	Low voltage-activated
mRNA	messenger RNA
mL	milliliter
mM	millimolar
mm	millimeter
mOsm/kg	milliosmole per kilogram
ms	millisecond
mV	millivolt
nM	nanomolar
NP	Asparagine, Proline
pA	picoampere
PCR	polymerase chain reaction
pF	picofarad
PIP_2	Phosphatidylinositol-4,5-biphosphate
pre-mRNA	precursor mRNA
qPCR	quantitative real-time PCR
RNA	ribonucleic acid
RNAi	RNA interference
SEM	standard error of the mean
SCA6	Spinocerebellar ataxia type 6
SSTR	Serine, Serine, Threonine, Arginine
VGCC	voltage-gated calcium channel
ω-Aga-IVA	ω-Agatoxin-IVA

Acknowledgements

Thank you to Dr. Terry Snutch for supervising my studies and for his guidance, advice and encouragement. I also thank my committee members Drs. Brian MacVicar, Yu Tian Wang and Vanessa Auld and external examiner Dr. Lynn Raymond for their valuable input and feedback.

Thanks to all past and present Snutch Lab members. I thank Dr. Esperanza Garcia for her help in the electrophysiological experiments including understanding of electrophysiological theories, protocol design and troubleshooting and the methods of analysis. Thank you to Dr. John Tyson for providing me with the clones and probes used in my experiments and for his help in the qPCR experiments and their analysis. Thank you to Dr. Stuart Cain for performing the dissections used for my qPCR experiments and his help in teaching of the electrophysiology technique. Thank you to Karen Jones for answering my questions and helping with various lab protocols. Additionally, I would like to thank Dr. Kirk Mulatz for teaching me basic laboratory techniques and trusting me to perform experiments as an undergrad!

Thank you to my wonderful family and friends for their endless love, support and encouragement throughout this process. To the friends I've been lucky enough to make along the way (the Neuroscience family and Botany girls) thank you for your friendship, support and advice.

Lastly, I thank you, the reader, for your interest in my work.

Dedication

Dedicated to my parents, Saman and Bilal, for their constant support and encouragement.

Chapter 1: Introduction

Calcium is an essential ion contributing to many cellular processes including gene regulation, muscle contraction, cell excitability and neurotransmitter release (Clapham, 2007; Simms and Zamponi, 2014). One route of calcium ion entry into cells is via voltage-gated calcium channels (VGCCs). VGCCs are a family of transmembrane proteins that activate upon depolarizations of the cell membrane and allow rapid calcium influx driven by an electrochemical gradient across the cell membrane. Diversity in VGCC biophysical properties, expression and modulation allows for the complex control of channel activity while retaining strict regulation of calcium levels. Genetic mutations in VGCCs cause dysfunction of VGCC activity which can lead to serious disorders of the nervous system (Lorenzon and Beam, 2000). Consequently, proper understanding of the complex impact of VGCCs on central nervous system (CNS) physiology and disease pathophysiology is essential in order to develop effective therapeutics and treatment options for VGCC-implicated disorders.

1.1 Voltage-gated calcium channels

VGCCs convert depolarizing changes in membrane potential into rapid increases in localized intracellular calcium concentrations (Lipscombe *et al.*, 2013). VGCCs can be generally categorized into two main groups; high voltage-activated (HVA) which require large depolarizations of the cell membrane in order to activate and low voltage-activated (LVA) which are activated by smaller depolarizations of the cell membrane that are closer to neuronal resting membrane potentials (Armstrong and Matteson, 1985; Simms and Zamponi, 2014). The main subunit that composes VGCCs is the α_1 subunit which contains most of the major functional

components of the channel including the ion-conducting pore, voltage sensor, gating machinery and most sites of modulation by drugs, toxins and second messengers (Catterall *et al.*, 2005).

The α_1 subunit is composed of four structurally homologous domains (I, II, III and IV) with each domain consisting of six transmembrane segments (S1-S6) (Figure 1.1). Positively charged residues in segment 4 (S4) of each domain enable it to serve as a voltage sensor for channel activation and are predicted to move outward following membrane depolarization to initiate a conformational change that opens the calcium-selective pore (Bezanilla, 2000; Catterall, 2000; Bezanilla, 2002; Catterall *et al.*, 2007; Catterall, 2010). The S5 and S6 segments along with the membrane-associated pore-loop (P-loop) connecting these segments form the pore lining of the channel and allow selectivity and permeation of calcium ions (Catterall, 2000).

The α_1 subunit of neuronal HVA calcium channels interacts with auxiliary β and $\alpha_2\delta$ subunits which modulate channel biophysical properties, second-messenger dependent regulation and trafficking (Figure 1.1) (Dolphin, 2012). The intracellular β subunit binds in the I-II cytoplasmic linker region of the α_1 subunit (Pragnell *et al.*, 1994). The α_2 and δ subunits are encoded by the same gene whose translated protein product is cleaved and subsequently disulfide-linked to yield the mature $\alpha_2\delta$ subunit (De Jongh *et al.*, 1990). Originally, the association of the $\alpha_2\delta$ subunit to the plasma membrane was thought to be due to the δ component being a transmembrane protein however more recent studies have provided evidence of a glycosylphosphatidylinositol (GPI) anchor attached to δ (Davies *et al.*, 2010). The interaction site(s) between the α_1 and $\alpha_2\delta$ subunits however are not yet fully understood (Dolphin, 2012). The skeletal muscle L-type VGCC is believed to also co-assemble with an additional subunit, γ , however whether this subunit also co-assembles with neuronal VGCCs has not yet been established (Catterall, 2000; Dolphin, 2012). Interestingly, while HVA channels have been

purified together with β and $\alpha_2\delta$ subunits and require their co-assembly in heterologous systems in order to conduct measurable currents, the LVA channels function well in heterologous systems with only an α_1 subunit (Catterall *et al.*, 2005).

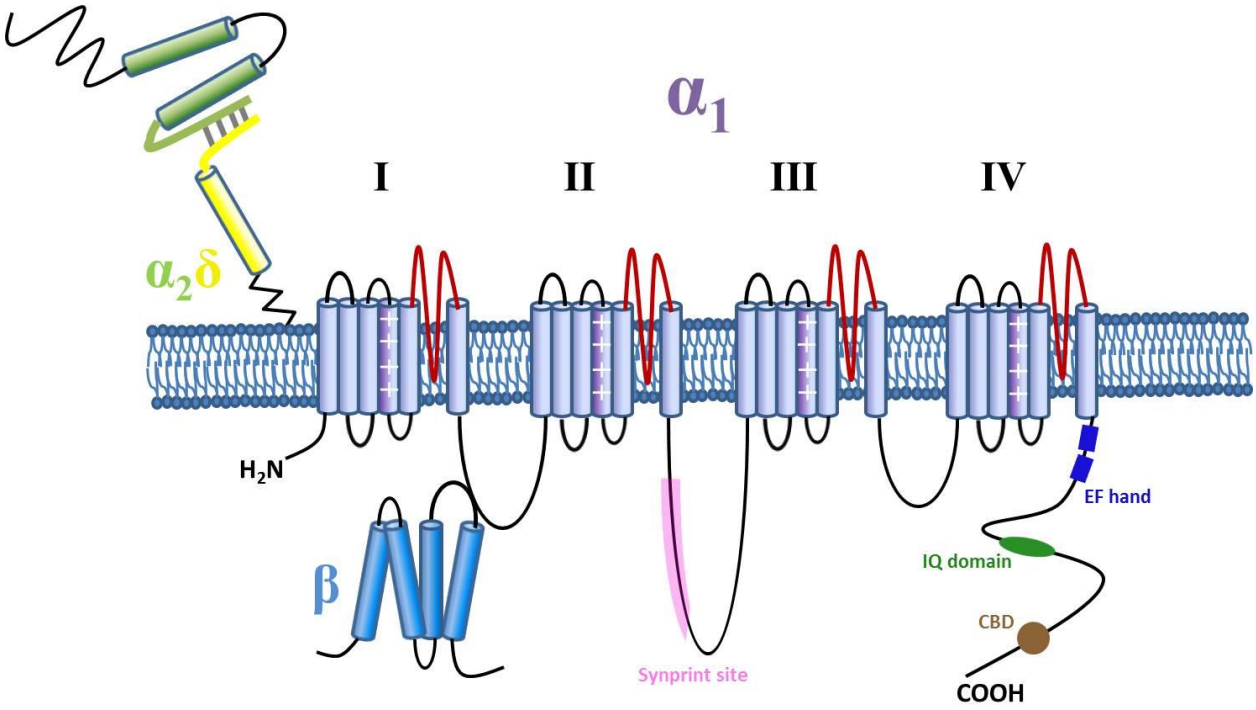

Figure 1.1: The proposed subunit composition of the $Ca_v2.1$ P/Q-type calcium channel
The α_1 subunit is composed of four homologous domains (labelled I, II, III and IV) with each domain consisting of six transmembrane segments. The S4 segments of each domain (dark purple shading with +) are the voltage sensors which sense depolarizations in the cell membrane and move outward resulting in a conformational change in the channel and thus channel activation . The S5 and S6 segments along with the P-loop (shown in red) connecting the segments make up the conduction pore which allows selectivity and permeation of calcium ions. The EF hand (dark blue rectangles), IQ domain (dark green ellipse) and calmodulin-binding domain (CBD) (brown circle) allow calcium-dependent regulation of the channel. The synprint site (pink) mediates interaction with synaptic vesicle and presynaptic membrane proteins. The intracellular β subunit (light blue) binds at the I-II intracellular linker and regulates kinetics and trafficking of the channel. The α_2 (light green) and δ (yellow) subunits are associated by disulfide bonds and the δ component is either attached to the membrane by a GPI-anchor (as shown in this figure) or is a transmembrane protein. The $\alpha_2\delta$ subunit has been shown to affect channel trafficking.

In mammals, there are ten different genes that encode the α_1 subunits of VGCCs and can be grouped into three major subfamilies; Ca_v1, Ca_v2 and Ca_v3 which differ in properties such as expression patterns, voltage-dependence, kinetics, conductance, modulation and pharmacology (Figure 1.2) (Ertel *et al.*, 2000).

The Ca_v1 subfamily includes four members; $Ca_v1.1$, $Ca_v1.2$, $Ca_v1.3$ and $Ca_v1.4$ all of which conduct L-type currents that are blocked by organic antagonists such as dihydropyridines, phenylalkylamines and benzothiazepines (Striessnig, 1999; Xu and Lipscombe, 2001; Catterall *et al.*, 2005). L-type channels are widely expressed in muscle and endocrine cells where they are involved in the initiation of contraction and secretion but are also found in many types of neurons and cardiac pacemaker cells (Catterall *et al.*, 2005).

The Ca_v2 subfamily includes three members; $Ca_v2.1$, $Ca_v2.2$ and $Ca_v2.3$ which conduct P/Q-type, N-type and R-type currents, respectively. These channels are predominantly expressed in neurons where they are involved in neurotransmission initiation at most fast synapses as well as calcium entry into dendrites and the soma (Catterall *et al.*, 2005). Ca_v2 channels are often distinguished by their sensitivities to specific polypeptide toxins isolated from the venom of spiders and marine cone snails (Mintz *et al.*, 1992b; Hillyard *et al.*, 1992; Catterall *et al.*, 2005).

The Ca_v3 subfamily consists of the LVA VGCCs and includes three members; $Ca_v3.1$, $Ca_v3.2$ and $Ca_v3.3$ all of which conduct T-type currents. They are expressed in many different cell types where their roles include shaping of action potentials and controlling repetitive firing patterns (Ertel *et al.*, 2000). Detailed pharmacology of these channels has not yet fully been determined although they are generally more sensitive to low concentrations of nickel compared to the HVA VGCCs (Perez-Reyes, 2003).

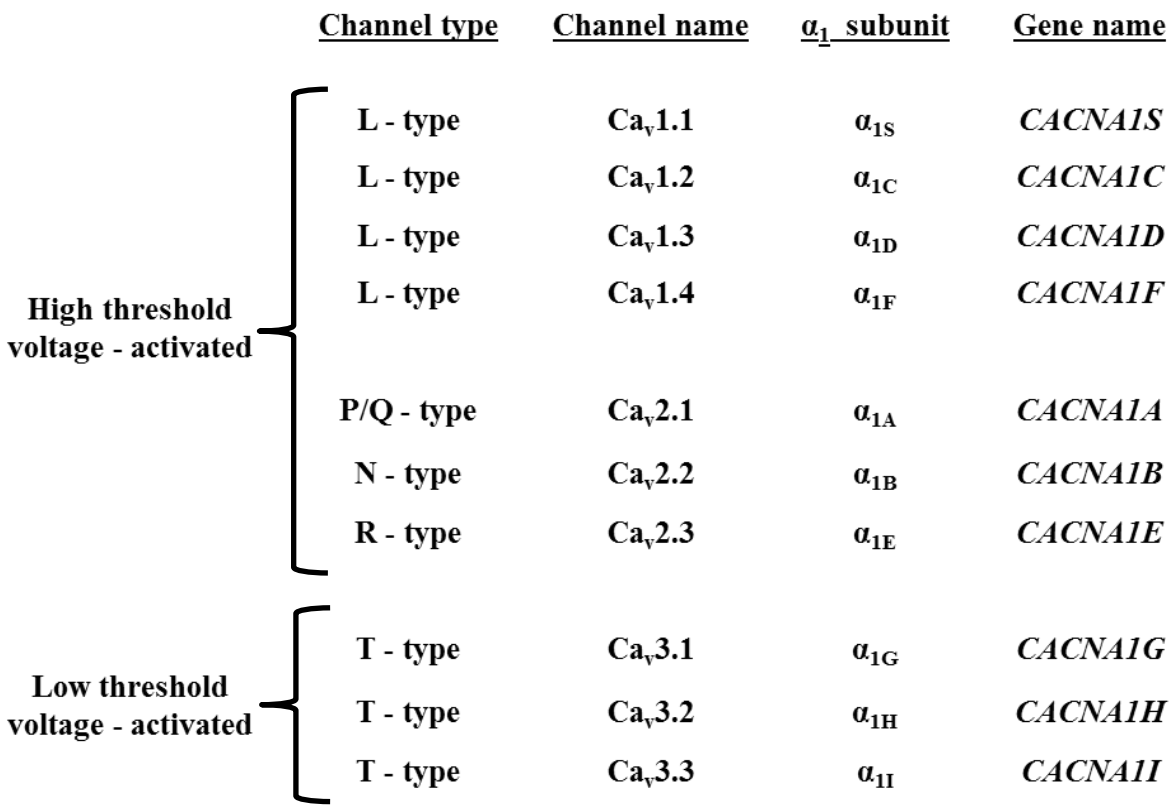

Figure 1.2: Diversity of voltage-gated calcium channels
There are two major categories of voltage-gated calcium channels (VGCCs), the high threshold voltage-activated (HVA) and low threshold voltage-activated (LVA) VGCCs. There are ten types of VGCCs encoded by different genes and can be divided into three major families: Ca_v1, Ca_v2 and Ca_v3. Each family contains multiple members that can differ in functional properties such as voltage-dependence, kinetics, modulation, expression and pharmacology.

1.2 $Ca_v2.1$ voltage-gated calcium channels

Mammalian $Ca_v2.1$ channels are encoded by the *CACNA1A* gene consisting of 47 exons (Ophoff *et al.,* 1996). $Ca_v2.1$ channels are widely expressed throughout the central nervous system (CNS) where they are essential for the initiation of neurotransmission (Takahashi and Momiyama, 1993; Westenbroek *et al.,* 1998). Consequently, mutations in the *CACNA1A* gene are known to cause serious disorders of the CNS (Ophoff *et al.,* 1996; Zhuchenko *et al.,* 1997). Pharmacologically, $Ca_v2.1$ channels are sensitive to blockade by the gating modifier peptide toxin ω-Agatoxin-IVA isolated from funnel web spider venom (Mintz *et al.,* 1992b; Adams, 2004). Co-assembly of $Ca_v2.1$ with different β subunits and modulation by distinct second-messenger pathways results in $Ca_v2.1$ currents displaying a variety of biophysical characteristics (Stea et al., 1994; Zamponi & Snutch, 1998). Further structural diversity is achieved by alternative splicing which in turn results in diverse functional effects across splice variant isoforms (Soong *et al.,* 2002). In particular, there are two main isoforms of $Ca_v2.1$ channels described in neurons, P- and Q-type, which differ in the type of current they conduct (P-type or Q-type current, respectively), their sensitivity to ω-Agatoxin-IVA and their spatial and temporal expression profiles (Randall and Tsien, 1995; Bourinet *et al.,* 1999).

1.2.1 Expression and physiological importance of $Ca_v2.1$ channels

$Ca_v2.1$ channels show a wide distribution throughout the rodent CNS including the hippocampus, spinal cord, cortex and brainstem and with their highest expression being in the cerebellum (Mori *et al.,* 1991; Starr *et al.,* 1991; Hillman *et al.,* 1991; Mintz *et al.,* 1992a; Stea *et al.,* 1994; Westenbroek *et al.,* 1998). Studies examining the subcellular distribution of $Ca_v2.1$ channels show that they are highly concentrated at presynaptic nerve terminals but are also

expressed post-synaptically in many dendrites and soma (Hillman *et al.,* 1991; Usowicz *et al.,* 1992; Westenbroek *et al.,* 1995; Day *et al.,* 1997; Westenbroek *et al.,* 1998). Reflective of their high concentration at presynaptic nerve terminals, $Ca_v2.1$ channels play an essential role in mediating neurotransmission in the CNS including the cerebellum, hippocampus, spinal cord, neuromuscular junction, cerebral cortex, striatum and calyx of Held (Uchitel *et al.,* 1992; Hillyard *et al,* 1992; Turner *et al.,* 1993; Takahashi and Momiyama, 1993; Luebke *et al.,* 1993; Regehr and Mintz, 1994; Wheeler *et al.,* 1994; Ishikawa *et al.,* 2005). Their somatodendritic expression is thought to mediate additional roles such as calcium-dependent gene expression, neural excitability, synaptic integration and plasticity and cell survival (Eilers *et al.,* 1996; Bayliss *et al.,* 1997; Magee *et al.,* 1998; Pineda *et al.,* 1998; Sutton *et al.,* 1999; Fletcher *et al.,* 2001).

A small region, the synprint site located in the II-III intracellular linker (Figure 1.1), in part mediates the channel's interactions with presynaptic membrane proteins syntaxin 1 and SNAP-25 as well as the vesicle membrane proteins synaptobrevin and synaptotagmin I (Rettig *et al.,* 1996; Martin-Moutot *et al.,* 1996; Kim and Catterall, 1997; Mochida *et al.,* 2003). These interactions allow the close coupling of the calcium source, $Ca_v2.1$, to the calcium sensor synaptotagmin I which induces vesicle fusion and neurotransmitter exocytosis upon the binding of two calcium ions (Charvin *et al.,* 1997). In addition to their physical interaction, these proteins can also regulate the activity and expression of one another. For example, when co-expressed separately in heterologous systems with $Ca_v2.1$ channels, both syntaxin and SNAP-25 decrease $Ca_v2.1$ channel availability by shifting the voltage-dependence of inactivation to more hyperpolarized membrane potentials (Bezprozvanny *et al.,* 1995; Zhong *et al.,* 1999). Further, when SNAP-25 is expressed alongside syntaxin-1A and synaptotagmin the inhibition of $Ca_v2.1$

activity is lifted suggesting that the formation of a "mature" snare complex reactivates $Ca_v2.1$ channels and thus enables an efficient mechanism of the calcium source near active zones with docked synaptic vesicles primed for release (Zhong *et al.,* 1999). At another level, it has been shown that selective influx through $Ca_v2.1$ channels activates expression of syntaxin-1A suggesting that a complex activity-dependent feedback mechanism allows $Ca_v2.1$ channels to play a role in the synaptic efficacy and proper functioning of the nervous system by regulation of synaptic activity (Sutton *et al.,* 1999).

1.2.2 $Ca_v2.1$ channelopathies

Given their widespread expression and their multiple roles in regulating synaptic activity, it is not surprising that mutations in $Ca_v2.1$ have been implicated in severe human neurological disorders. Mutations in the *CACNA1A* gene encoding the α_1 subunit of $Ca_v2.1$ channels have been shown to cause serious neurological disorders in humans, termed "channelopathies," and include familial hemiplegic migraine type 1 (FHM1), episodic ataxia type 2 (EA2) and spinocerebellar ataxia type 6 (SCA6) which can often have overlapping symptoms (Ophoff *et al.,* 1996; Zhuchenko *et al.,* 1997). $Ca_v2.1$ channels are also implicated in the neurological disease Lambert-Eaton myasthenic syndrome wherein VGCC autoantibodies show a preference for $Ca_v2.1$ channels resulting in a reduction in neurotransmitter release and other symptoms including motor weakness (Pinto *et al.,* 2002).

Familial hemiplegic migraine type 1

Familial hemiplegic migraine type 1 (FHM1) is a rare, autosomal-dominant disorder that is classified as a subtype of migraine with aura. Migraine with aura is characterized by recurring

attacks of unilateral headaches that may be preceded by an aura phase consisting of additional transient neurological sensations. The defining characteristic of FHM1 is the additional symptom of motor weakness during the aura phase. Additionally, based on the type of FHM1 mutation, some FHM1 patients exhibit cerebellar symptoms such as progressive cerebellar ataxia, nystagmus or cerebellar atrophy (Ophoff *et al.,* 1996; Pietrobon, 2010). The aura phase is thought to be due to cortical spreading depression (CSD), a slowly propagating wave of intense neuronal and glial depolarization along the cortex (Lauritzen, 1994). The headache component begins with activation of trigeminal sensory afferents which activate trigeminovascular neurons in the trigeminal nucleus caudalis and thalamic nuclei which further activate areas of the brainstem and forebrain involved in processing of pain and additional migraine symptoms (Pietrobon, 2013). The initiation of either the CSD or headache components are still not fully understood but it has been hypothesized that CSD triggers initiation of the headache (Bolay *et al.,* 2002; Moskowitz *et al.,* 2004). The 21 distinct FHM1 mutations identified thus far are all missense mutations generally located in important functional regions of the $Ca_v2.1$ channel including the voltage sensors and pore lining regions (Pietrobon, 2010). Studies conducted on FHM1 mutations show overall gain-of-function effects on $Ca_v2.1$ channel properties such as increased channel open probability and single channel calcium influx, mainly as a result of a shift in channel activation to lower voltages and faster activation kinetics (Hans *et al.,* 1999a; Tottene *et al.,* 2002; Tottene *et al.,* 2005; Catterall *et al.,* 2008; Pietrobon, 2013; Di Guilmi *et al.,* 2014).

Episodic ataxia type 2

Episodic ataxia type 2 (EA2) is a rare disorder characterized by sudden attacks of cerebellar dysfunction displayed by ataxic gait, limb incoordination, slurring and nystagmus (Pietrobon, 2010). More than 50 different EA2 mutations have been reported so far with the majority of them being either nonsense mutations or mutations that disrupt the open reading frame causing truncations of the protein leading to an overall decrease in the amount of functional channels (Pietrobon, 2010). The EA2 missense mutations identified thus far are predominantly located in the pore forming regions of the channel and show overall loss-of-function effects due to a shift in the current-voltage relationship to more positive potentials, enhanced channel inactivation, slower recovery from inactivation, decreased current density and/or decreased trafficking of channels to the plasma membrane (Wappl *et al.,* 2002; Spacey *et al.,* 2004; Imbrici *et al.,* 2004; Wan *et al.,* 2005; Pietrobon, 2010; Rose *et al.,* 2014).

Spinocerebellar ataxia type 6

Spinocerebellar ataxia type 6 (SCA6) is a late-onset neurodegenerative ataxic disorder of the cerebellum that generally progresses slowly and can be preceded by gaze-evoked nystagmus, dysarthria, imbalance and vertigo (Jodice *et al.,* 1997; Kordasiewicz and Gomez, 2007; Giunti *et al.,* 2015). SCA6 is caused by small polyglutamine (polyQ) expansions, encoded by CAG trinucleotide repeats at the C-terminus of *CACNA1A* (Zhuchenko *et al.,* 1997). Interestingly, although $Ca_v2.1$ channels are expressed in both Purkinje and granule cells of the cerebellum, SCA6 pathophysiology shows a preference for the loss of Purkinje cells while granule cells are relatively spared (Ishikawa *et al.,* 1999; Kordasiewicz and Gomez, 2007; Tsunemi *et al.,* 2008). Whether SCA6 falls into the category of channelopathy or polyQ disorder is a somewhat

controversial topic with evidence for both sides (Frontali, 2001; Giunti *et al.,* 2015). For example, some studies have shown that CAG expansions affect $Ca_v2.1$ functional properties and cause shifts in the voltage-dependences of activation and inactivation, alterations in the rate of inactivation and impairment of G protein-dependent regulation (Matsuyama *et al.,* 1999; Toru *et al.,* 2000; Restituito *et al.,* 2000). In contrast, studies performed on dissociated Purkinje cells from knock-in mice with CAG expansions have reported no effects on channel properties suggesting that the depletion of Purkinje cells is more in line with polyQ diseases wherein cytotoxic aggregation of polyQ-containing protein is thought to trigger a yet to be fully characterized cell death pathway (Ishikawa *et al.,* 1999; Saegusa *et al.,* 2007; Watase *et al.,* 2008; Gatchel and Zoghbi, 2005).

1.2.3 Modulation of $Ca_v2.1$ channels

Diversity in $Ca_v2.1$ properties can be achieved by the co-assembly of its α_1 subunit with any of the four different isoforms of each auxiliary β (β_1-β_4) and $\alpha_2\delta$ ($\alpha_2\delta_1$-$\alpha_2\delta_4$) subunits (Dolphin, 2012). In general, $Ca_v2.1$ channel activity is dramatically increased when co-expressed with β and $\alpha_2\delta$ subunits (Mori *et al.,* 1991). All isoforms of the β subunit increase the current amplitude and overall whole-cell current however different isoforms have diverse effects on the inactivation kinetics and voltage-dependence, most likely resulting from the differences in their binding affinities to the $Ca_v2.1$ α_1 subunit (Stea *et al.,* 1994; De Waard and Campbell, 1995; DeWaard *et al.,* 1995). Of note, the $\alpha_2\delta$ subunit has been shown to control the number of $Ca_v2.1$ channels localized at presynaptic terminals by affecting channel trafficking (Hoppa *et al*., 2012).

$Ca_v2.1$ channels also undergo two different types of calcium-dependent feedback modulations due to a complex interaction involving calcium-binding to calmodulin (CaM)

through an IQ-domain, EF-hand motif and CaM-binding domain (CBD) (Figure 1.1) (Lee *et al.,* 1999; Christel and Lee, 2012). Calcium-dependent facilitation (CDF) is a rapid activity-dependent enhancement of channel opening while calcium-dependent inactivation (CDI) is a subsequent, slower process of channel inactivation following calcium influx (Chang *et al.,* 2007).

G proteins have also been shown to directly inhibit $Ca_v2.1$ channels, with activation of G-protein-coupled receptors causing a decrease in peak current amplitude and slowing of activation and inactivation kinetics (Zamponi and Snutch, 1998). Studies have shown that this occurs through the binding of the $G_{\beta\gamma}$ subunit to the I-II linker region of the channel (Herlitze *et al.,* 1996; De Waard *et al.,* 1997). This G-protein-dependent inhibition of $Ca_v2.1$ channels can be relieved by high frequency trains of action potentials (Brody *et al.,* 1997).

1.2.4 The ω-Agatoxin-IVA peptide toxin

The 48 amino acid peptide toxin ω-Agatoxin-IVA (ω-Aga-IVA) is isolated from the venom of the funnel web spider, *Agelenopsis aperta,* and shows high selectivity for $Ca_v2.1$ channels (Mintz *et al.,* 1992b; Adams, 2004). The P- and Q-type isoforms of $Ca_v2.1$ however display different sensitivities for the toxin (Mintz *et al.,* 1992b; Randall and Tsien, 1995; Adams, 2004). Native P-type $Ca_v2.1$ channels have a higher sensitivity for ω-Aga-IVA with an IC_{50} of ~1 nM whereas Q-type $Ca_v2.1$ channels have a lower sensitivity to ω-Aga-IVA with an IC_{50} of ~90 nM (Randall and Tsien, 1995).

The mechanism by which ω-Aga-IVA inhibits $Ca_v2.1$ currents is not through direct blocking of the channel pore but rather by the altering of the voltage-dependence of channel gating, classifying it as a gating modifier (McDonough *et al.,* 1997b). ω-Aga-IVA stabilizes the closed state of $Ca_v2.1$ channels with respect to the open state, thereby making voltages that

normally activate the channel too weak to activate ω-Aga-IVA-bound channels (McDonough, 2007). It is thought that ω-Aga-IVA binds to the S3-S4 linker of domain IV and "traps" the S4 voltage sensor in the inward, resting position thereby preventing channel activation (McDonough, 2007; Catterall *et al.*, 2007). Application of strong depolarizations results in the unbinding of ω-Aga-IVA from bound channels relieving channel blockade (McDonough 1997b). ω-Aga-IVA can also affect $Ca_v2.1$ channel kinetics including slowing of channel activation and acceleration of channel deactivation (McDonough, 2007).

1.3 Alternative splicing

An important mechanism that allows for substantial diversity in $Ca_v2.1$ channel characteristics is alternative splicing (Lipscombe *et al.*, 2013). Splicing is the process of converting precursor mRNA (pre-mRNA) into mature mRNA that can then be directly translated into protein. Non-coding regions (introns) are recognized and removed from the pre-mRNA by the spliceosome protein complex (Hoskins and Moore, 2012). Spliceosome activity is influenced by the intron sequence, spliceosome composition and various splicing factors. Alterations in the choice of splice sites utilized can produce different mRNA sequences which generate considerable protein diversity (Black, 2003).

There are multiple patterns of alternative splicing that can occur. One type of splicing is where there is exclusion or inclusion of an entire cassette exon (Figure 1.3A). A second type involves mutual exclusion between two or more adjacent exons wherein only one exon out of the group is included in the final mRNA sequence (Figure 1.3B). Third and fourth types of alternative splicing occur when alternative 5' (Figure 1.3C) or 3' (Figure 1.3D) splice sites allow either the lengthening or shortening of the preceding or following exon. A fifth type is by the use

of alternative 5' promoters (Figure 1.3 E) and a sixth type is by the use of alternative 3' polyadenylation cleavage sites (Figure 1.3 F). Lastly, an intron present in the pre-mRNA can evade the splicing process and be retained in the mature mRNA sequence (Figure 1.3G). Of note, the final mRNA sequence can be a product of a combination of the different alternative splicing patterns described (Black, 2003).

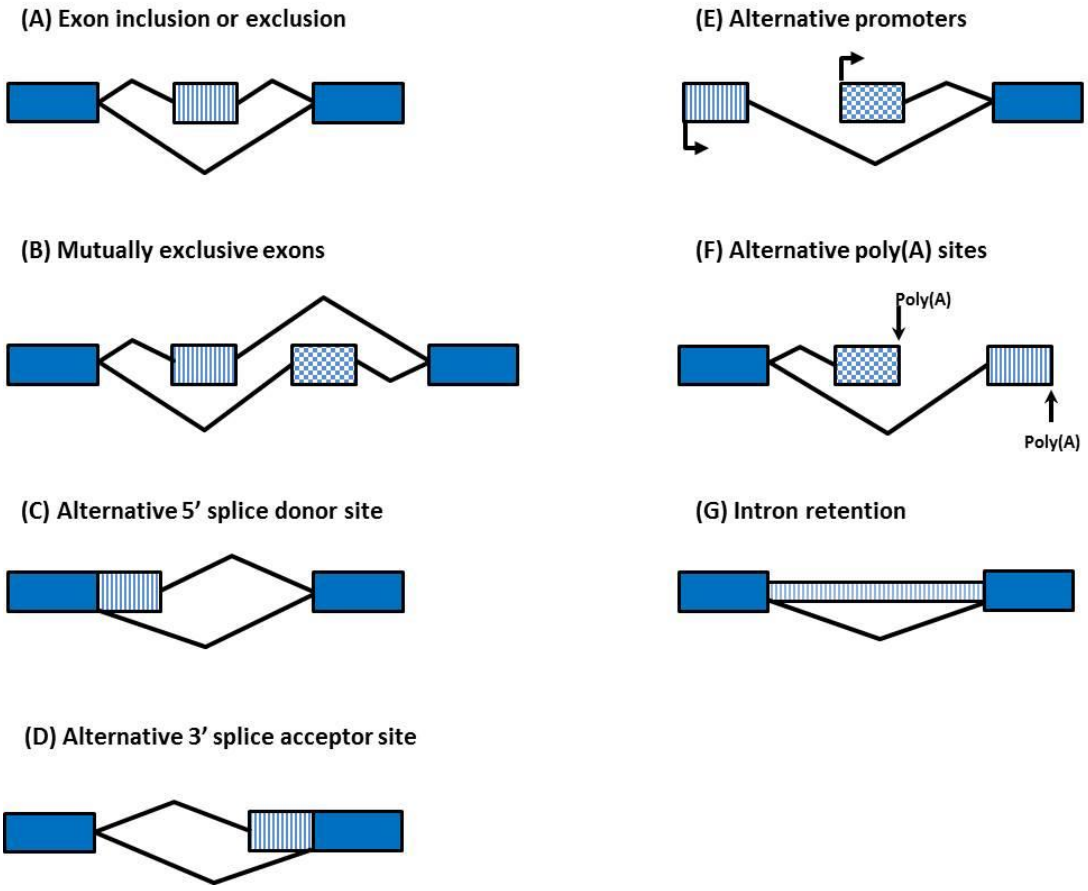

Figure 1.3: Patterns of alternative splicing
Alternative splicing of pre-mRNA can occur by a variety of different patterns leading to distinct mature mRNAs. This schematic summarizes the known variations of alternative splicing. Exons are shown as blue rectangles and alternative exons are shown as striped or checkered rectangles. **(A)** A cassette exon can be included or excluded **(B)** A group of exons can be mutually excluded **(C)** Alternative 5' donor sites **(D)** Alternative 3' acceptor sites **(E)** Alternative promoters which are shown as bent arrows. **(F)** Alternative poly(A) cleavage sites **(G)** An intron can be retained in the final mRNA sequence. Mature mRNA transcripts can be a result of a combination of the various alternative splicing patterns. Figure adapted with permission from Annual Reviews (Black, 2003).

1.3.1 Alternative splicing of $Ca_v2.1$ channels

A number of both rodent and human $Ca_v2.1$ splice variants have been discovered and many exhibit differential expression throughout the CNS. Additionally, due to the location of changes in important functional regions of the channel many result in significant effects on channel biophysical and pharmacological properties (Bourinet *et al.,* 1999; Krovetz *et al.,* 2000; Soong *et al.,* 2002; Chaudhuri *et al.,* 2004).

One site of alternative splicing is located at the beginning of exon 10 in the intracellular loop connecting domains I and II (Figure 1.4; #1). Here, there can be an insertion of both a valine and glycine (10; +VG), insertion of only a glycine (Δ10A; +G) or no insertion of either amino acid (Δ10B; designated "-") resulting from alternative splice acceptor sites (Figure 1.3D) (Bourinet *et al.,* 1999; Soong *et al.,* 2002). The +VG variant is found at approximately 17% abundancy in human cerebellum with the remaining 83% consisting of the Δ10A (+G) and Δ10B (-) variants combined (Soong *et al.,* 2002). The valine insertion (+VG) has been shown to slow channel inactivation kinetics and enhance both G-protein-dependent inhibition and PKC-dependent upregulation when compared to the glycine insertion alone (+G) (Bourinet *et al.,* 1999).

A second site of alternative splicing is found in segment 6 of domain II where exons 16 and 17 can be either included (+16/17) or excluded (-16/17) in an exon inclusion/exclusion manner (Figure 1.3A) (Figure 1.4; #2). Interestingly, although the -16/17 variant was identified during transcript scanning of $Ca_v2.1$ cDNA fragments it has not been detected in cDNA from human cerebellum with the +16/17 variant being present in 100% of transcripts (Soong *et al.,* 2002).

A third splicing site is located in the intracellular loop connecting domains II and III where there can be inclusion (+VEA; 17) or exclusion (-VEA; Δ17A) of the tripeptide VEA due to alternative donor sites at the 5' end of intron 17 (Figure 1.3C) (Figure 1.4; #3). A majority of transcripts from human cerebellum lacked the VEA insertion with the –VEA variant having an abundancy of ~99% (Soong *et al.,* 2002).

A further site is located in the extracellular loop between segment 3 and 4 in domain IV. Here, there can be either inclusion (+NP; +31*) or exclusion (-NP; -31*) of exon 31 which encodes the dipeptide NP (Figure 1.3A) (Figure 1.4; #4). This site is of significant importance as the inclusion or exclusion of NP is the determining factor for the Q-type or P-type classification of $Ca_v2.1$ channels, respectively. Insertion of NP (i.e. Q-type currents) shifts the V_{50} of activation to more positive potentials (Bourinet *et al.,* 1999). More notably, the Q-type isoform has a significantly lower sensitivity to ω-Agatoxin-IVA than the P-type with k_d values of 100 nM and 2 nM, respectively (Bourinet *et al.,* 1999). Their expression can also differ between cell type, for example the P-type (-NP) isoform is predominantly expressed in cerebellar Purkinje cells whereas the Q-type (+NP) isoform is more highly expressed in granule cells (Randall and Tsien, 1995; Bourinet *et al.,* 1999). In human cerebellum the +NP variant was found to be present in 95% of $Ca_v2.1$ transcripts (Soong *et al.,* 2002).

Another splice site can be found at the proximal end of the C-terminal protein tail region where there is mutual exclusion of two different versions of exon 37, exon 37a or 37b which results in the channel possessing either of two possible versions of an EF-hand motif (EFa or EFb, respectively) (Figure 1.3B) (Figure 1.4; #5) (Soong *et al.,* 2002). The EF-hand contains calcium binding sites that are important for the calcium-dependent regulation of $Ca_v2.1$ channels. The presence of the EFa-hand motif allows both calcium-dependent facilitation (CDF) and

calcium-dependent inactivation (CDI) whereas presence of the EFb-hand motif greatly suppresses CDF but leaves CDI unaffected (Chaudhuri *et al.,* 2004). Whole brain mouse samples show predominant EFb expression overall. In mouse and rat cerebellum samples however there is an early developmental switch from predominantly EFb to predominantly EFa expression during the first 1-2 weeks following birth (Chang *et al.,* 2007). Interestingly, a developmental switch in expression in human cerebellum from predominantly EFa to EFb was only seen in males between the ages of 30 and 40 years with cerebellum samples from females showing mostly EFb expression at all ages (Chang *et al.,* 2007).

A sixth site is located closer to the C-terminus where there can be inclusion or exclusion of exons 43 and 44 in all four possible combinations (43±/44±) due to two exon inclusion or exclusion splicing events (Figure 1.3A) (Figure 1.4; #6) (Krovetz *et al.,* 2000; Soong *et al.,* 2002). Although the 43+/44+ variant is found in more than 90% of cDNA from human cerebellum, its abundancy in other regions such as the amygdala, cerebral cortex, hippocampus, hypothalamus, thalamus and substantia nigra is reduced to approximately equal proportions as the 43+/44- variant (Soong *et al.,* 2002). The 43-/44- variant also shows a significant amount of variation in its expression between different brain regions with a range of 2-26% abundancy whereas the 43-/44+ variant exhibits low abundance in all regions examined. Inclusion of exon 43+ has been shown to produce significantly larger currents than the 43- variant suggesting that it may play a role in the regulation of trafficking channels (Soong *et al.,* 2002). The inclusion of the 44+ exon has been shown to increase the rate of channel inactivation when compared with 44- variant channels (Krovetz *et al.,* 2000).

Another splice region occurs at the distal end of the C terminus where as a result of alternative acceptor sites (Figure 1.3D) there can be insertion of a pentanucleotide (GGCAG)

which causes a frame shift leading to full translation of exon 47 (+47) rather than an in-frame stop codon which results in a shorter C-terminal tail (Δ47) (Figure 1.3D) (Figure 1.4; #7) (Soong *et al.,* 2002). Analysis of adult human cortex RNA shows expression levels of 79% and 21% for the +47 and Δ47 variants whereas in human cerebellum the values are 65% and 35%, respectively (Soong *et al.,* 2002; Adams *et al.,* 2009). The Δ47 variant has been shown to have a faster rate of recovery from inactivation and less accumulation of inactivation during tonic depolarizations than the +47 variant (Adams *et al.,* 2009).

In the intracellular linker of domain II and III, two splice variants that have large deletions in the synprint site with deletion lengths of 193 (Δ1) and 154 (Δ2) amino acids have been identified from whole rat brain samples (Figure 1.4; #8) (Rajapaksha *et al.,* 2008). The Δ1 variant shows a decrease in whole-cell currents and a shift in the voltage-dependence of inactivation to more depolarized voltages whereas Δ2 does not seem to have any detectable differences when compared with the full-length synprint site variant. Both variants show wide distribution throughout the rat brain with the Δ1 variant having a significantly higher expression than Δ2 in all regions except for the hippocampus.

1.3.2 The +SSTR splice variant

Most recently, the +SSTR $Ca_v2.1$ splice variant, which encodes the insertion of four amino acids (SSTR) in the S3-S4 linker of domain III, has been identified (Figure 1.4; #9) (Allen *et al.,* 2010; Snutch Lab unpublished data). The +SSTR splice variant has been found present in whole brain mouse and rat samples with an abundancy of 10% and 24%, respectively (Allen *et al.,* 2010; Snutch Lab unpublished data). The expression of the +SSTR splice variant in isolated CNS regions has yet to be reported. Additionally, the biophysical and pharmacological properties

of the +SSTR and ΔSSTR $Ca_v2.1$ splice variants have not yet been compared. As previous studies have shown substantial effects of alternative splicing on $Ca_v2.1$ channel characteristics, we wanted to define the potential differences in expression and functional properties between the +SSTR and ΔSSTR splice variants.

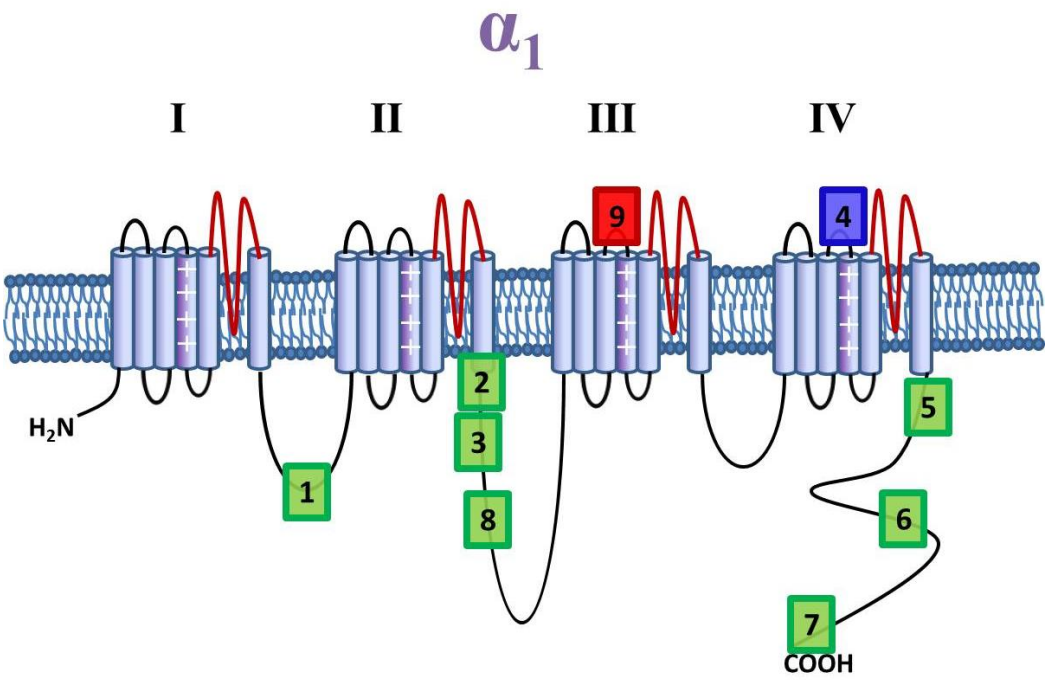

Figure 1.4: Sites of alternative splicing of $Ca_v2.1$ identified in rat and human CNS
This figure shows the location of some of the alternative splice variants that have been identified in either human or rat CNS samples.

(1) Insertion of either +VG (10) or +G (Δ10A) or no insertion of either amino acid (Δ10B).
(2) Inclusion (+16/17) or exclusion (-16/17) of exons 16 and 17.
(3) Inclusion (17) or exclusion (Δ17A) of the tripeptide VEA.
(4) Inclusion (+NP) or exclusion (-NP) of exon 31.
(5) Mutual exclusion of exons 37a or 37b resulting in the EFa or EFb isoform of the EF-hand motif, respectively.
(6) Inclusion or exclusion of exons 43 and 44 (43±/44±).
(7) Full length translation of C-terminus (+47) or inclusion of an in-frame stop codon resulting in a shorter C-terminus (Δ47).
(8) Deletions in the synprint site with lengths of either 193 (Δ1) or 154 (Δ2) amino acids or no deletions.
(9) Inclusion (+SSTR) or exclusion (ΔSSTR) of four amino acids (SSTR).
(Soong *et al.*, 2002; Rajapaksha *et al.*, 2008; Allen *et al.*, 2010)

1.4 Thesis hypotheses and significance of project

1.4.1 Hypotheses

Previous studies on $Ca_v2.1$ splice variants have shown that their expression levels can vary significantly between different regions of the mammalian CNS. The +SSTR splice variant has been found to be present in whole brain rodent samples however its relative expression in different regions of the CNS has yet to be studied.

1. **I hypothesized that the +SSTR and ΔSSTR splice variants are differentially expressed in the rat central nervous system.** In order to test this hypothesis, I performed splice variant-specific analysis using quantitative real-time PCR on samples dissected from ten different regions of the adult male Sprague Dawley rat central nervous system.

Alternative splicing in key functional regions of the $Ca_v2.1$ channel have been shown to significantly affect channel properties such as voltage-dependence and kinetics. The SSTR insertion site is in close proximity to the domain III S4 voltage sensor that contributes to channel gating in response to depolarizations and may result in it differentially affecting channel biophysical properties in different brain regions.

2. **I hypothesized that the inclusion or exclusion of SSTR differentially affects the biophysical properties of the channel.** In order to test this hypothesis, I performed whole-cell patch-clamp electrophysiology on HEK 293 cells transiently transfected with $Ca_v2.1$ cDNA that included or excluded SSTR.

The NP insertion in the S3-S4 linker of domain IV has been shown to disrupt ω-Agatoxin-IVA binding causing a significant decrease in sensitivity of $Ca_v2.1$ currents to the toxin (Bourinet *et al.,* 1999). However, it has been suggested that the other three channel domains could also be involved in the toxin's mechanism of action as all four domains need to move upon depolarization in order for the channel to activate (Winterfield and Swartz, 2000). The SSTR insertion site in the S3-S4 linker of domain III is in a homologous region as the NP insertion site and may also affect ω-Agatoxin-IVA binding.

3. **I hypothesized that the inclusion or exclusion of SSTR can affect the sensitivity of $Ca_v2.1$ channels to ω-Agatoxin-IVA.** To test this hypothesis I performed whole-cell patch-clamp electrophysiology to compare the sensitivity of the +SSTR and ΔSSTR variants to ω-Agatoxin-IVA.

1.4.2 Significance of project

Previous studies investigating alternative splicing of $Ca_v2.1$ channels show significant differences in the expression of splice variants throughout the CNS and on functional properties of the channel. This diversity in expression and properties due to alternative splicing is thought to provide fine-tuning of $Ca_v2.1$ channel activity and modulation that fulfills physiological functions in specific types of cells and tissues as well as for different types of stimuli (Krovetz *et al.,* 2000; Liao *et al.,* 2009). This allows for efficiency and regulatory complexity of $Ca_v2.1$-mediated processes throughout the CNS. Examining the expression profiles and biophysical properties of the +SSTR and ΔSSTR splice variants would help towards understanding their specific roles and importance in CNS physiology.

Additionally, although $Ca_v2.1$ channels are widely distributed throughout the CNS, mutations in the channel cause different types of disorders that manifest in selected CNS regions. This spatial localization of pathophysiology is thought to be influenced by the contextual expression of alternative splice variants and their diverse effects on channel properties together with the nature of individual mutations (Adams *et al.,* 2009; Liao *et al.,* 2009). Splice variant-specific disease pathology can occur in two ways. Firstly, a mutation can be located in an alternatively spliced exon that is either included or excluded in the mature mRNA. As a result, the severity of disease pathology in a specific cell or tissue will be dependent on the level of expression of the mutation-containing alternative exon. For example, EA2 premature stop codon mutations that are only located in the alternatively spliced EFa exon cause loss of $Ca_v2.1$ current mediated by EFa-containing channels but leave EFb-containing channels unaffected (Graves *et al.,* 2008). Additionally, the CAG expansions seen in SCA6 are only able to form in the +47 variant of $Ca_v2.1$ channels which is the predominant variant expressed in Purkinje cells of SCA6 patients where selective degeneration of Purkinje cells causes the symptoms exhibited in SCA6 (Tsunemi *et al.,* 2008).

The second mechanism of splice variant-specific disease effects is by mutations causing differential effects on channel properties based on the splice variant included in the channel. For example, FHM1 mutations show more pronounced effects on the voltage-dependent properties of channels containing the Δ47 rather than the +47 variant (Adams *et al.,* 2009). Furthermore, the CAG expansions seen in SCA6 only cause a negative shift in the voltage-dependence of inactivation of $Ca_v2.1$ channels when expressed with the –NP variant (which is predominantly expressed in Purkinje cells) and may explain the Purkinje cell-specific depletion in SCA6 whereas +NP variant-expressing granule cells are unaffected (Toru *et al.,* 2000). Additionally,

the dramatic loss-of-function effects caused by EA2 mutations are only exhibited in the +47 variant of $Ca_v2.1$ channels which are dominantly expressed in human cerebellum (Jeng *et al.,* 2006). As such, investigating the expression of the +SSTR and ΔSSTR variants in specific CNS regions could provide insight into their potential influence in $Ca_v2.1$-related disorders.

Furthermore, in order to develop effective therapeutics for $Ca_v2.1$-implicated disorders, investigation of the pharmacological properties of splice variants is necessary as alternative splicing can significantly affect channel pharmacology. For example, the sensitivity to ω-Aga-IVA between the +NP and –NP splice variants of $Ca_v2.1$ are dramatically different (Bourinet *et al.,* 1999). Therefore, comparing the effects of ω-Aga-IVA on current block between the +SSTR and ΔSSTR variants will clarify whether +SSTR-containing $Ca_v2.1$ channels are potential targets for therapeutics developed based on the structural properties of ω-Aga-IVA.

Chapter 2: The +SSTR and ΔSSTR Variants are Differentially Expressed Throughout the Rat Central Nervous System

2.1 Introduction

Ten distinct genes encode the primary α_1 subunit of voltage-gated calcium channels that differ in characteristics such as biophysical properties, pharmacology, modulation and expression (Ertel *et al.,* 2000). Further diversity of VGCCs is achieved through the process of alternative splicing through which different mRNA and consequently different protein sequences can be generated from the same gene (Black, 2003). It has been suggested that each gene encoding the α_1 subunit has the potential to produce thousands of unique splice isoforms due to the influence of cell-specific splicing factors (Lipscombe *et al.,* 2013). Alternative splicing in key functional regions of the $Ca_v2.1$ channel can lead to significant differences in the channel's kinetics, voltage-dependence, modulation and pharmacology (Bourinet *et al.,* 1999; Soong *et al.,* 2002; Chaudhuri *et al.,* 2004; Adams *et al.,* 2009). Furthermore, the level of expression of $Ca_v2.1$ splice variants can vary significantly between different CNS regions and cell types (Randall and Tsien, 1995; Soong *et al.,* 2002).

$Ca_v2.1$ channels play an essential role in neurotransmission throughout the CNS and alternative splicing is thought to be a mechanism by which $Ca_v2.1$ activity can be specialized in order to satisfy specific cell or tissue conditions and various types of signals or stimuli (Krovetz *et al.,* 2000; Liao *et al.,* 2009). As such, the region-specific expression levels of splice variants provide initial insights into the potential impact the variants have towards CNS physiology and possibly disease pathophysiology.

Abundancy of the +SSTR variant of $Ca_v2.1$ has been previously shown to be ~10% and ~24% in whole brain mouse and rat, respectively (Allen *et al.,* 2010; Snutch Lab unpublished data). A more thorough examination of its expression in more defined CNS regions has not yet been conducted. We hypothesized that the abundance of the +SSTR and ΔSSTR variants would likely vary across different regions of the CNS and differ significantly from the whole brain abundancy values previously reported.

To test this hypothesis, I performed quantitative real-time PCR on ten different regions of the adult Sprague Dawley rat central nervous system using ΔSSTR- and +SSTR-specific probes. I found that in contrast to whole rat brain RNA, the +SSTR variant is in significantly greater abundance than ΔSSTR in the brainstem, reticular thalamus and spinal cord. Additionally, I was curious to see whether there is an association between the expression of the +SSTR and -NP variants as it has been theorized that they may be regulated by the same splicing factor (Allen *et al.,* 2010). Therefore, I also performed qPCR on the same ten regions using +NP- and –NP-specific probes and found that in regions where +SSTR is in greater abundance than ΔSSTR, the –NP variant is significantly more abundant than +NP suggesting similar splicing regulatory mechanisms might exist for the +SSTR and –NP splice variants.

2.2 Methods

2.2.1 Dissections, RNA isolation and cDNA generation

Ten different CNS regions of three adult (P120) male Sprague Dawley rats (Charles River Laboratories; CD 001) were dissected independently. The regions studied were; brainstem, cerebellum, occipital cortex, reticular thalamus, sensory thalamus, caudate putamen, frontal cortex, hippocampus, somatosensory cortex and spinal cord. Following dissection, samples were

immediately immersed in TRI Reagent Solution (Ambion; AM9738) and homogenized by pipetting in TRI Reagent Solution approximately 10x the volume of the sample. Samples were stored in a -80^{o}C freezer until further use. RNA was extracted from samples using the MagMax-96 for Microarrays Kit (Ambion; AM1839) and cDNA was generated using the Applied Biosystems™ High Capacity cDNA Reverse Transcription Kit (Fisher Scientific; 4368814). The cDNA synthesis thermocycler procedure was 25^{o}C for 10 minutes, 37^{o}C for 120 minutes and 85^{o}C for 5 seconds with holding at 4^{o}C using a 2720 Thermal Cycler (Applied Biosystems).

2.2.2 Quantitative real-time PCR procedure and probes

The qPCR reactions were set up in triplicates using KAPA PROBE FAST qPCR Master Mix (2x) (KAPA Biosystems; KM4702) in hard-shell 384-well PCR plates (Bio-Rad Laboratories; HSP3805). The qPCR probes contained FAM at the 3' end, BkFQ quencher at the 5' end and a ZEN quencher between the 9th and 10th base. Probes were designed by Dr. John Tyson and made by Integrated DNA Technologies (Table 2-1). The machine used for detection was the C1000 Touch Thermal cycler CFX384 Touch^{TM} Real-Time (PCR Detection) System (Bio-Rad). Run protocol: 95^{o}C for 3 minutes, (95^{o}C for 15 seconds, 60^{o}C for 45 seconds) x 40.

Table 2.1: Sequences for qPCR probes.

Variant	Forward Primer	Reverse Primer	Probe sequence
ΔSSTR	GGACTTCATAGTGG TCAGTGG	GACTTGATGGTGTTGA TGTCC	CTTTGCCTTCACTGGCAAT AGCAAAGG
+SSTR	GGACTTCATAGTGG TCAGTGG	GACTTGATGGTGTTGA TGTCC	TTCACGAGCAGTACACGTG GCAAT
–NP	GTCACCGAGTTTGG GAATAAC	CGGAGGAGTTTGATGA GTCG	ACCTGAGCTTTCTCCGCCT CTTC
+NP	CAGCATCACAGACA TCCTCG	CGGAGGAGTTTGATGA GTCG	ACCGAGTTTGGGAATCCGA ATAACTTCATC

2.2.3 Analysis of qPCR data

Quantification cycle (C_q) values were obtained using the Bio-Rad CFX Manager version 3.1 (Bio-Rad Laboratories) and were normalized to GAPDH. Amounts of each variant were averaged between the triplicates and a ratio was calculated by dividing the "alternative" variants (i.e. +SSTR and +NP) by the respective "reference" variants (i.e. ΔSSTR and –NP). Ratios were then averaged between the three different animals to generate Figure 2.1 which shows the values of the ratios of +SSTR/ΔSSTR (Figure 2.1A) and +NP/–NP (Figure 2.1B) (± SEM) with the "reference" variants (i.e. ΔSSTR and –NP) set at 1.

2.3 Results

2.3.1 The +SSTR and ΔSSTR variants are differentially expressed in the rat CNS

In order to generate regional expression profiles, I performed quantitative real-time PCR using different probes for the +SSTR and ΔSSTR splice variants in ten different regions of the adult male Sprague Dawley rat CNS. Figure 2.1A shows the expression ratio of the +SSTR variant relative to ΔSSTR (+SSTR/ΔSSTR) with ΔSSTR values for each region set at 1. I found that the brainstem, reticular thalamus and spinal cord show significantly higher expression levels of +SSTR relative to ΔSSTR with +SSTR/ΔSSTR ratios of 2.15 ± 0.19, 1.56 ± 0.11 and 2.28 ± 0.78, respectively.

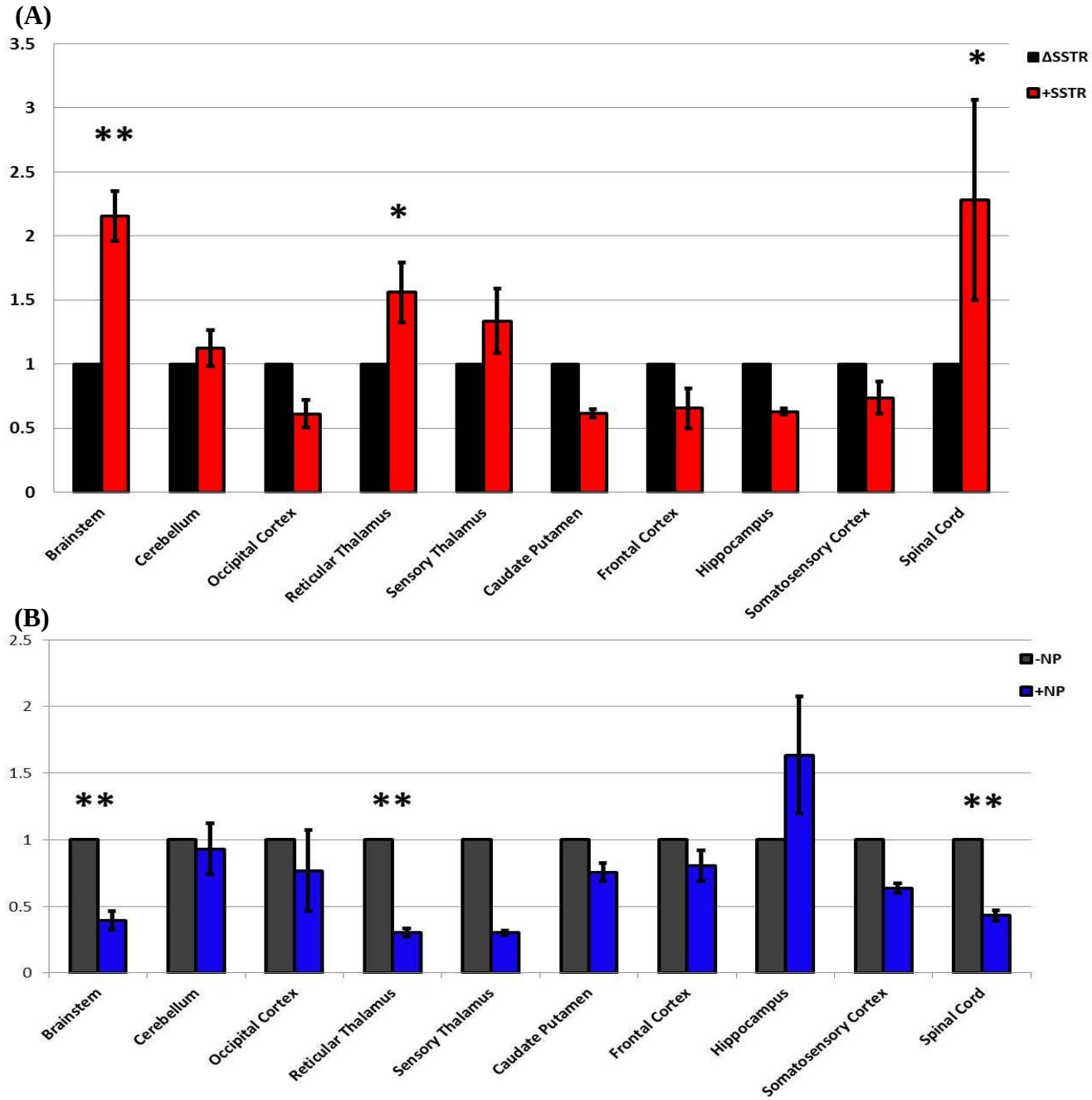

Figure 2.1: The +SSTR splice variant is differentially expressed throughout the rat CNS
Averaged C_q values acquired in triplicates from qPCR performed using splice variant-specific probes were normalized to GAPDH C_q values to obtain the amount of each variant in the CNS region sample. Ratios were calculated by dividing "alternative" variants (i.e. +SSTR and +NP) by their respective "reference" variants (i.e. ΔSSTR and –NP) and averaged between the three different male adult Sprague Dawley rats. Bar graphs in this figure show the mean ratios (± SEM) with the "reference" variants set at 1. **p<0.01, *p<0.05 (one-way ANOVA). **(A)** Ratio of +SSTR relative to ΔSSTR showing significantly higher expression of +SSTR in the brainstem, reticular thalamus and spinal cord. **(B)** Ratio of +NP relative to –NP showing that regions where +SSTR is in greater abundance –NP is significantly more expressed than +NP.

2.3.2 CNS regions with higher +SSTR expression levels mostly express –NP

In order to determine whether there was an association between +SSTR and –NP expression I also performed qPCR using +NP and –NP specific probes. Figure 2.1B shows +NP splice variant expression relative to the –NP expression (+NP/–NP) with –NP values for each region set at 1. Of note, in the regions where +SSTR is more abundant than ΔSSTR (the brainstem, reticular thalamus and spinal cord) the –NP splice variant is in much greater abundance than +NP with +NP/–NP ratios of 0.39 ± 0.07, 0.30 ± 0.03 and 0.43 ± 0.04, respectively. Although –NP is overall in greater abundance in all regions studied except for the hippocampus, a substantial lower amount of transcripts containing the +NP insertion is seen in the brainstem, reticular thalamus and spinal cord.

2.4 Discussion

Performing qPCR using splice variant-specific probes on different regions of the rat CNS, I found that +SSTR is the more abundant variant in a subset regions of the rat CNS including the brainstem, reticular thalamus and spinal cord (Figure 2.1A). This is in contrast to previous results from whole brain rat RNA that showed +SSTR abundancy of ~24% and demonstrates that studies performed on whole brain do not necessarily provide an accurate representation of splice variant expression. This most likely is a result of whole brain samples mainly being composed of cortical tissue which may mask the expression levels of variants in smaller brain regions.

The neuron-specific alternative splicing factor Nova-2 protein is expressed throughout the CNS and has been previously shown to enhance the expression of transcripts including +SSTR (Yang *et al.* 1998; Ule *et al.*, 2006; Allen *et al.*, 2010). Nova-2 binds to pre-mRNA

YCAY clusters and either represses or enhances inclusion of the target alternative splice exon depending on whether it binds upstream or downstream, respectively (Ule *et al.,* 2006; Allen *et al.,* 2010). Approximately 10% of $Ca_v2.1$ transcripts from wild-type whole mouse brain RNA contain +SSTR whereas Nova-2 knockout mice show no detectable amounts of +SSTR-containing transcripts suggesting that Nova-2 has an enhancing action on +SSTR insertion (Allen *et al.,* 2010). In regions where +SSTR is predominantly expressed, Nova-2 might be in greater abundance and/or more active resulting in increased +SSTR transcripts. Alternatively, exon selection is often influenced by the collaborative action of several different splicing factors and it is possible that the SSTR splicing site is regulated by multiple splicing factors (Lipscombe *et al.,* 2013). For example, members of the RNA-binding FOX and polypyrimidine tract-binding (PTB) splicing factor families have been shown to regulate alternative splicing of many other types of VGCCs (Tang *et al.,* 2009; Tang *et al.,* 2011; Gehman *et al.,* 2011).

In comparing the expression profiles of +SSTR and –NP, I uncovered an association between the two splice variants with areas wherein +SSTR is more abundant also having a much greater abundancy of the –NP variant. These results support a previous study that suggested Nova-2 enhances +SSTR insertion and suppresses NP insertion thus favoring the +SSTR and –NP combination of $Ca_v2.1$ channels (Allen *et al.,* 2010). While suggestive, the notion of an association between +SSTR and –NP is speculative as these data are from specifically amplified PCR products. More appropriately, the examination of full-length $Ca_v2.1$ transcripts would provide a clearer picture of the exact contextual combinations of native $Ca_v2.1$ channel splice variants.

It is also important to keep in mind that this study was only conducted on samples from adult male rats and that previous studies have demonstrated that $Ca_v2.1$ splice variant expression

can significantly vary depending on gender and developmental stages (Chaudhuri *et al.,* 2004; Chaudhuri *et al.,* 2005; Chang *et al.,* 2007).

In summary, the results from this study show that the +SSTR variant is predominantly expressed in certain regions of the CNS supporting the hypothesis that +SSTR and ΔSSTR channels may possess distinct functional properties important for proper $Ca_v2.1$ channel-mediated signaling in specific regions. Furthermore, the predominant expression of +SSTR in certain regions may influence the localized pathophysiology of $Ca_v2.1$-implicated disorders. For example, studies have shown that FHM1 mutations can exert different levels of functional impact on channel properties between alternative splice variants (Adams *et al.,* 2009). As such, in the future it would be of particular importance to compare the effects of FHM1 mutations on +SSTR variant channels as they are highly expressed in the brainstem and thalamus which are thought to be involved in FHM1 pathophysiology (Pietrobon, 2010; Park *et al.,* 2014).

Chapter 3: Effects of +SSTR and ΔSSTR on the Biophysical Properties of $Ca_V2.1$ Channels

3.1 Introduction

VGCCs are activated upon depolarizations of the cell membrane allowing the rapid influx of calcium ions (Catterall, 2000). The gating of VGCCs relies on the movement of the S4 voltage sensors of each domain in response to depolarization which results in conformational changes that drive activation (Bezanilla, 2000; Bezanilla, 2002; Catterall *et al.,* 2007; Catterall, 2010). Alternative splicing in key functional domains has previously been shown to significantly alter the gating and biophysical properties of the $Ca_v2.1$ channel (Bourinet *et al.,* 1999; Krovetz *et al.,* 2000; Soong *et al.,* 2002; Rajapaksha *et al.,* 2008; Adams *et al.,* 2009). This diversity in $Ca_v2.1$ properties is thought to be the mechanism by which complexity and fine-tuning of $Ca_v2.1$-mediated processes such as neurotransmitter release at CNS synapses can occur (Krovetz *et al.,* 2000; Lipscombe, 2013)

The +SSTR splice variant includes the insertion of four amino acids in the S3-S4 extracellular linker of domain III which is in close proximity to the S4 voltage sensor. We hypothesized that SSTR insertion could potentially affect the biophysical properties of the channel including voltage-dependence and kinetics of channel activation and inactivation. I performed whole-cell patch-clamp electrophysiology on HEK 293 cells transfected with either the ΔSSTR and +SSTR $Ca_v2.1$ splice variants (together with auxiliary subunits β_4 and $\alpha_2\delta_1$). The results showed that channels containing the +SSTR have faster activation kinetics and more hyperpolarized V_{50act} and $V_{50inact}$ values than the ΔSSTR splice variant channels.

Furthermore, we studied the impact of the differences in biophysical properties between the splice variants on their response to different action potential waveforms (APWs). I analyzed currents elicited by APWs with different durations and found an increase in charge transference through +SSTR containing channels that was substantially less sensitive to APW broadening than ΔSSTR channels. This difference in APW response between the two splice variants as a result of their unique biophysical properties suggests each variant could have distinct roles in processing different types of action potentials.

3.2 Methods

3.2.1 Cell culture maintenance and transfections

Human embryonic kidney (HEK) 293 cells were grown in Dulbecco's Modified Eagle's Medium (Life Technologies; 12800-082) that was supplemented with 10% heat-inactivated fetal bovine serum (Sigma Aldrich; F1051) and 1% Gibco® MEM non-essential amino acids (Life Technologies; 11140-050). Cells were maintained in a humidified water-jacketed incubator at 37^{o}C with 5% CO_2. Cells were seeded at 15-20% confluency on 12mm sterile glass coverslips (Marienfeld Superior; 0111520) that were coated with 0.1mg/mL poly-D-lysine hydrobromide (Sigma-Aldrich; P7886). The following day, cells were transiently transfected with full-length human $Ca_v2.1$ cDNA that was either ΔSSTR or +SSTR along with the auxiliary subunits β_4 and $\alpha_2\delta_1$ and eGFP reporter plasmid in a 1:1:1:0.5 molar ratio using Turbofect Transfection Reagent (Thermo Scientific; R0531). The splice variants present in the full-length $Ca_v2.1$ cDNA (pTPS 3063) were: +G, +16/17, -VEA, -NP, 37a, +43, +44 and -47. The cDNA and Turbofect were mixed together in opti-MEM® I Reduced Serum Medium (Life Technologies; 31985070) and incubated for 13 minutes at room temperature before being applied to the cells.

3.2.2 Electrophysiological recordings

The day following transfection, the whole-cell patch-clamp electrophysiology technique was performed in order to record macroscopic barium currents. The internal pipette solution contained 105mM CsCl, 25mM TEACl, 11mM EGTA, 10mM HEPES, 5mM Mg-ATP and 1mM $CaCl_2$ (pH 7.2 adjusted with CsOH and osmolality 290 mOsm/kg adjusted with D-mannitol). The 5mM barium external solution contained 87.5mM CsCl, 40mM TEACl, 10mM HEPES, 10mM glucose, 5mM $BaCl_2$ and 1mM $MgCl_2$ (pH 7.4 adjusted with TEAOH and osmolality 310 mOsm/kg adjusted with D-mannitol). Borosilicate glass patching pipettes (Sutter Instrument; BF 150-86-10) were prepared using a horizontal puller (Sutter Instrument; Model P-97) and fire polished using a microforge (Narishige; MF-900). Pipette resistances were between 2 and 5 MΩ when containing internal solution. The bath for the external solution was grounded with an Ag/AgCl Disc electrode (Warner Instruments; 64-1314, E242). The liquid junction potential was calculated with Clampex software version 9.0 (Axon Instruments) using the mobility, valence and concentration of each ion in the internal and bath solutions and was found to be 1.1mV at room temperature (25^{o}C). Reported voltages have not been corrected for the junction potential. Current recordings were acquired using an Axopatch 200B amplifier (Molecular Devices) with Clampex software version 9.0 (Axon Instruments) and filtered at 2 kHz bandwidth. Series resistance was compensated by 70% and whole cell parameters were turned off during recordings. Data were acquired using a Digidata 1322A (Molecular Devices) interface and were analyzed using Clampfit software version 9.0 (Axon Instruments) and Origin software version 8.6 (OriginLab Corporation). Recordings were performed at room temperature.

3.2.3 Electrophysiological recording protocols and data analysis

Current-voltage relationships were studied by applying a series of 260 millisecond depolarizing test pulses at membrane potentials ranging from -50 mV to +45 mV in 5 mV increments from a holding potential of -90 mV (Figure 3.1A). Peak currents were plotted as a function of membrane potential and were fit with the modified Boltzmann equation $I_m = [G_{max}(V_m-E_{rev})]/[1+ e^{[(Vm-V50)/k]}]$ where G_{max} is the maximum slope conductance, V_m is the test membrane potential, E_{rev} is the extrapolated reversal potential, V_{50act} is the membrane potential at which 50% of the channels are activated and k_{act} is the slope factor of activation which reflects voltage sensitivity (Figure 3.2A). Goodness of fit R^2 values were ≥ 0.998. V_{50act} and k_{act} were analyzed using one-way ANOVA at significant levels of 0.01 and 0.05, respectively. Cells with current density less than 20pA/pF were omitted from calculations. Extrapolated reversal potentials were used to calculate conductances in order to generate activation curves which were fit with the Boltzmann equation $I/I_{max}=A2 + (A1-A2)/[1+e^{[(Vm-V50act)/kact]}]$ where I_{max} is the maximum current, V_{50act} is the membrane potential at which 50% of the channels are activated and k_{act} is the slope factor of activation (Figure 3.2B).

The kinetics of activation (τ_{act}) were measured by fitting the peak current trace from the IV protocol recordings with a standard single exponential function $I=Ae^{-t/\tau}$, where A is the current amplitude and τ is the time constant.

The degree of inactivation was measured by calculating the residual current for each test pulse. Residual current was calculated by dividing the remaining current at the end of the test pulse by the peak current value for the same test pulse (Figure 3.4B).

Voltage-dependence of inactivation was studied using a steady-state inactivation protocol which consisted of a 5 second conditioning pre-pulse at membrane potentials ranging from -120

mV to +10 mV with 10 mV increments followed by an 80 ms test pulse at 0 mV (Figure 3.5A). Current obtained from the test pulse was plotted as function of the conditioning pre-pulse membrane potential (Figure 3.6A). The data was fit with the Boltzmann equation $I/I_{max}=A2 + (A1-A2)/[1+e^{[(Vm-V50inact)/kinact]}]$ where I_{max} is the maximum current, $V_{50inact}$ is the membrane potential at which 50% of the channels are inactivated and k_{inact} is the slope factor of inactivation. Goodness of fit R^2 values were ≥ 0.998. $V_{50inact}$ and k_{inact} were analyzed using one-way ANOVA at the 0.05 significance level.

To study whether the differences in voltage-dependence and kinetics between the splice variants could affect their response during an action potential waveform (APW) I tested three different APWs with half-durations of 0.60 ms, 1.5 ms and 3.5 ms and a holding potential of -80 mV (top graph in Figure 3.7A). The APW half-duration (also referred to as "half-width" or "half-height width") represents the width of the APW at the half-maximal of the spike amplitude and is commonly used to measure spike width (Bean, 2007). The original APW used in this study was recorded from a Purkinje neuron and given to Snutch lab by Dr. David Yue. Charge transference was calculated by integrating the area under the current trace. Values from the longer APWs (i.e. 1.5 ms and 3.5 ms) were divided by the values from the shortest APW (i.e. 0.6 ms) of that cell in order to determine the relative changes in charge transference due to increasing APW duration.

3.3 Results

3.3.1 The SSTR insertion affects the voltage-dependence of $Ca_v2.1$ activation

Whole-cell patch-clamp electrophysiology was performed using a current-voltage (IV) relationship protocol to study biophysical properties including voltage-dependence of activation

and kinetics of channel activation and inactivation (Figure 3.1A). Figures 3.1B and 3.1C show representative traces of barium currents obtained using the IV protocol for the ΔSSTR and +SSTR splice variants, respectively.

Figure 3.2A shows the IV curve generated by plotting the normalized peak current from each test pulse as a function of membrane potential with ΔSSTR shown in black and +SSTR shown in red. The IV curve was fit with the modified Boltzmann equation to get the V_{50act} which corresponds to the membrane potential at which half of the channels are activated and the Boltzmann slope factor k_{act} which represents voltage sensitivity. I found a 4.9 mV difference in V_{50act} with the +SSTR splice variant having a more hyperpolarized V_{50act} than the ΔSSTR (V_{50act} in mV = -19.56 ± 0.29 and -14.66 ± 0.44, respectively). There was also a small but statistically significant difference in the k_{act} between the two splice variants with the +SSTR variant showing a slightly lesser sensitivity to voltage than ΔSSTR (k_{act}= -4.85 ± 0.08 and -4.56 ± 0.10, respectively). Activation curves seen in Figure 3.2B were generated from the extrapolated reversal potentials from the IV curves and were fit with the Boltzmann equation.

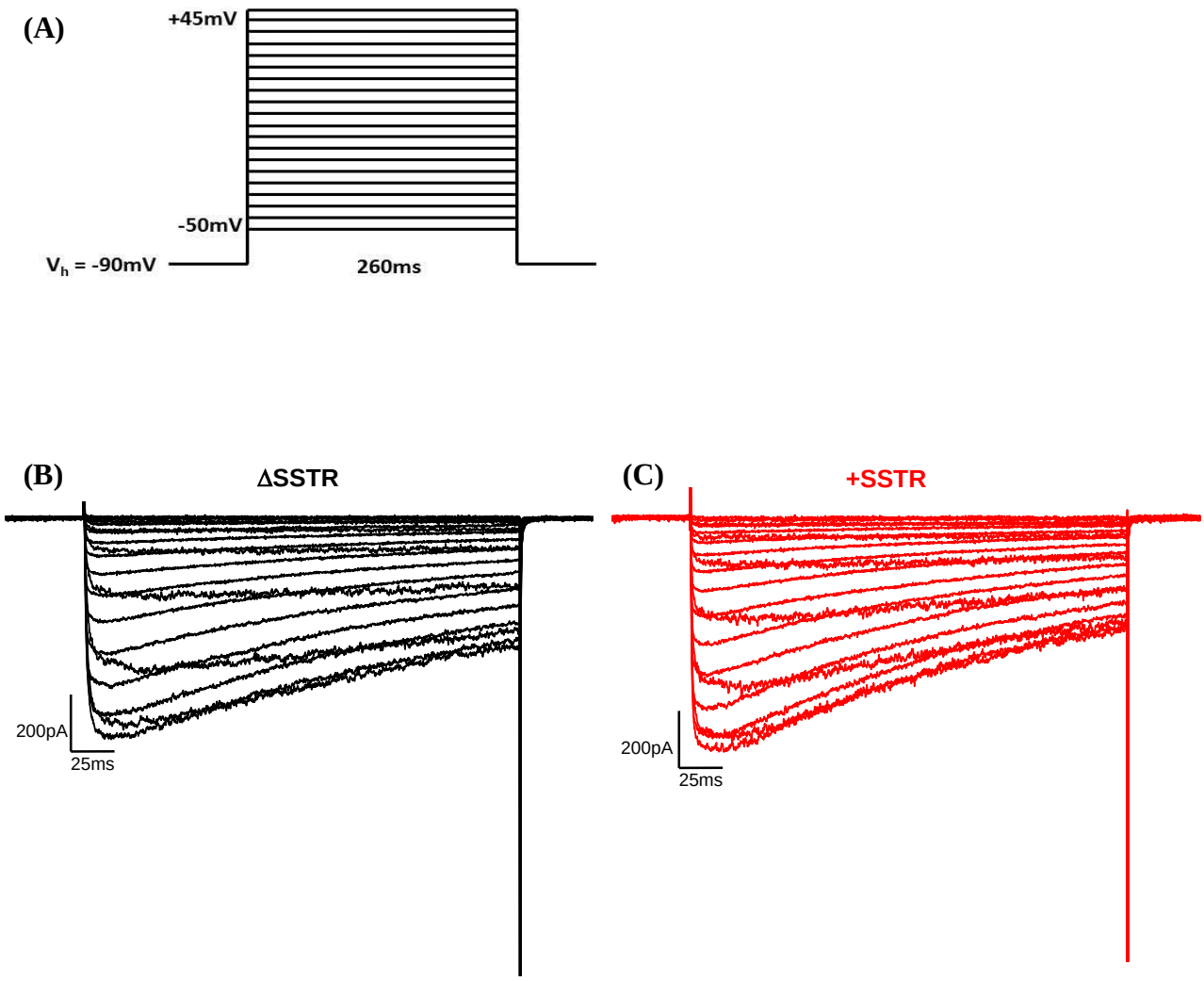

Figure 3.1: Current-voltage protocol and current waveforms of the ΔSSTR and +SSTR $Ca_v2.1$ splice variants

Barium currents were evoked using a current-voltage (IV) protocol in order to study the current-voltage relationship of the two splice variant isoforms. **(A)** The IV protocol consisted of 260 ms test pulses ranging from -50 mV to +45 mV in 5 mV increments from a holding potential of -90 mV that were applied every seven seconds. **(B)** and **(C)** Representative barium current traces of ΔSSTR and +SSTR $Ca_v2.1$ splice variants elicited by the IV protocol, respectively.

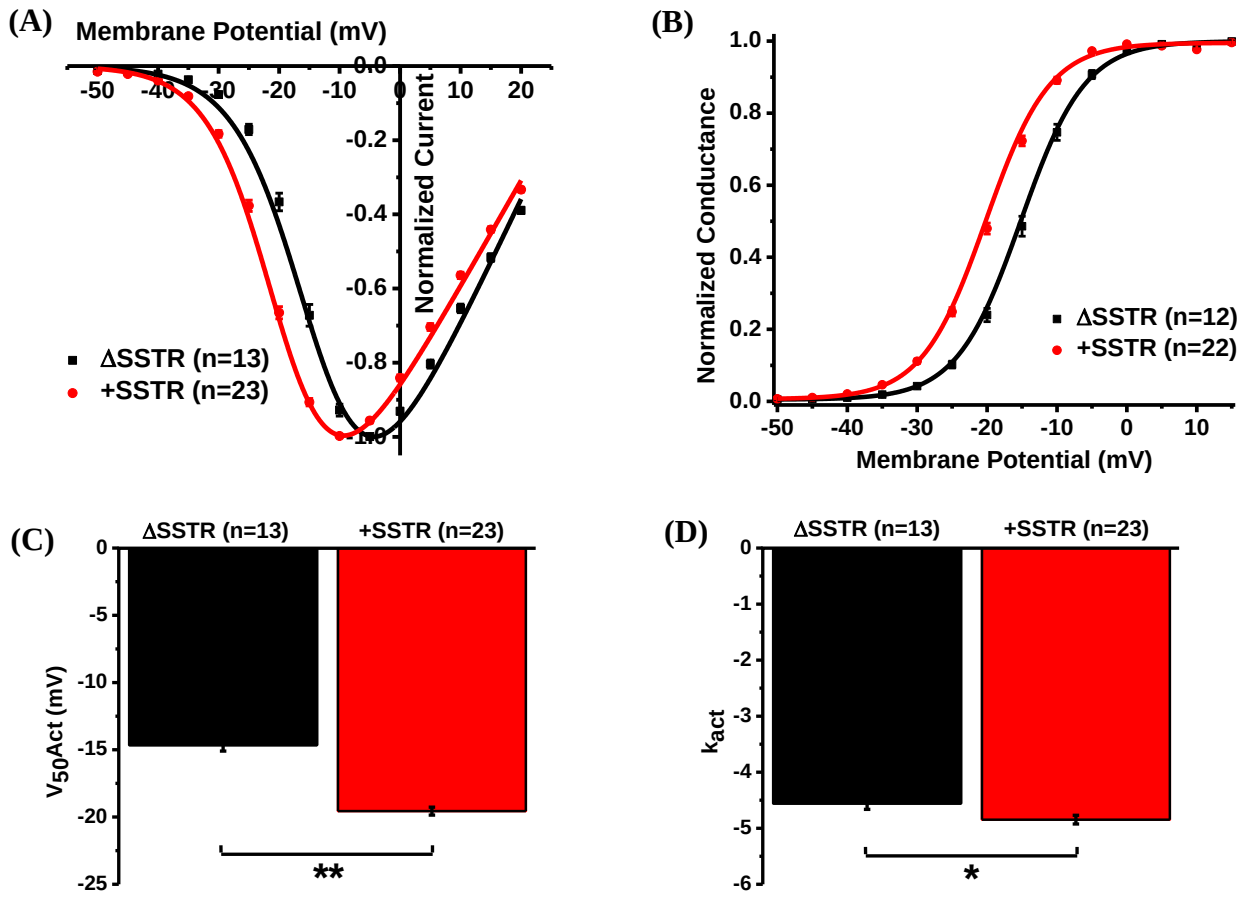

(E)

	V_{50} act ± SEM (mV)	k_{act} ± SEM
ΔSSTR (n=13)	-14.66 ± 0.44	-4.56 ± 0.10
+SSTR (n=23)	-19.56 ± 0.29**	-4.85 ± 0.08*
**Significant at 0.01 level. *Significant at 0.05 level.		

Figure 3.2: SSTR affects the voltage-dependence of activation of $Ca_v2.1$
(A) IV curves for the ΔSSTR (black) and +SSTR (red) $Ca_v2.1$ splice variants were generated by plotting the normalized peak current value at each test pulse as a function of the membrane potential. Data were fit with the modified Boltzmann equation. **(B)** Activation curves for ΔSSTR (black) and +SSTR (red) were generated from the extrapolated reversal potentials from fitting of the IV curve. Activation curves were fit with the Boltzmann equation. **(C)** Bar graph showing mean V_{50act} values (±SEM) with +SSTR having a more hyperpolarized V_{50act} than ΔSSTR. **(D)** Bar graph displaying mean k_{act} values (±SEM) showing that +SSTR has lower voltage sensitivity than ΔSSTR. **(E)** Table showing mean values of V_{50act} and k_{act} (±SEM). **p<0.01; *p<0.05 (one-way ANOVA).

3.3.2 The SSTR insertion affects the activation kinetics of $Ca_v2.1$

To determine the effects of +SSTR on the activation kinetics of the channel, the peak current trace obtained from the IV protocol for each cell was fit with a single exponential function to obtain the time constant of activation (τ_{act}). I found a 0.35 ms difference in the τ_{act} between the $Ca_v2.1$ splice variants with the +SSTR splice variant having faster activation kinetics than the ΔSSTR variant (τ_{act} in ms= 1.25 ± 0.09 and 1.60 ± 0.13, respectively) (Figures 3.3A, B, C).

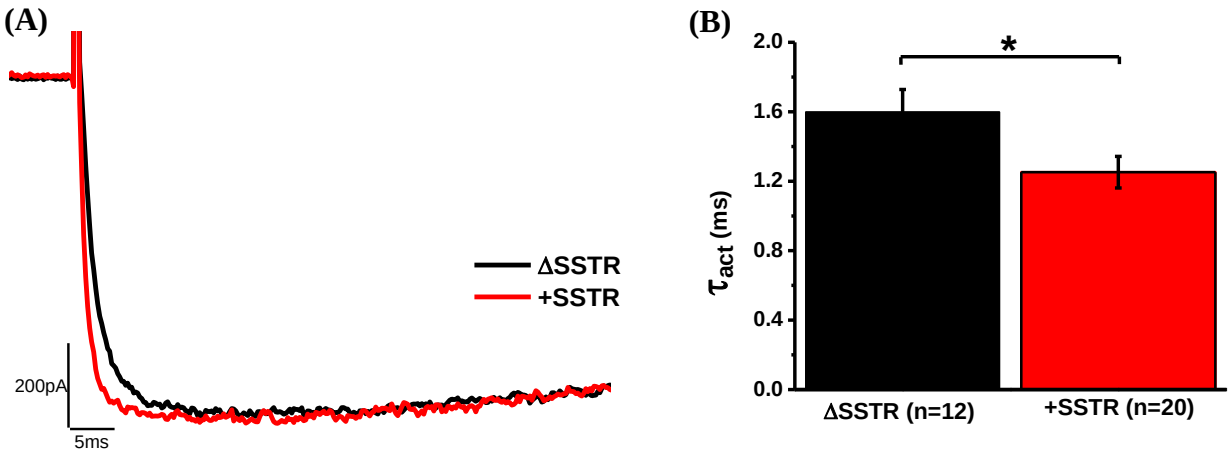

(C)

	τ_{act} ± SEM (ms)
ΔSSTR (n=12)	**1.60 ± 0.13**
+SSTR (n=20)	**1.25 ± 0.09**
***Significant at 0.05 level.**	

Figure 3.3: SSTR affects $Ca_v2.1$ activation kinetics
(A) Overlapped representative peak barium current traces of ΔSSTR (black) and +SSTR (red) demonstrating the faster activation kinetics of +SSTR relative to ΔSSTR. Peak currents were fit with a single exponential function in order to obtain the activation time constant (τ_{act}). **(B)** Bar graph showing mean τ_{act} values (±SEM) with +SSTR having a smaller τ_{act} and thus faster activation kinetics than ΔSSTR. **(C)** Table showing mean values of activation time constants (±SEM)**.** *p<0.05 (one-way ANOVA).

3.3.3 The SSTR insertion does not affect the degree of $Ca_v2.1$ inactivation

The inactivation time constant could not be determined due to the very slow inactivation of $Ca_v2.1$ current in barium external solution (Figure 3.4A). As an alternative method to study potential differences in the inactivation kinetics between the splice variants, I calculated the residual current. The residual current provides the degree of inactivation that occurs during the duration of a prolonged test pulse. For currents elicited by the IV protocol test pulses, residual current can be calculated by divided the remaining current at the end of the 260 ms test pulse by the peak current value from the same test pulse (Figure 3.4B). I calculated the residual current for test pulses between -25 mV and 20 mV and found no significant difference in the amount of inactivation between the two splice variants suggesting that there is unlikely to be a significant difference in the inactivation kinetics between the channel isoforms (Figure 3.4C).

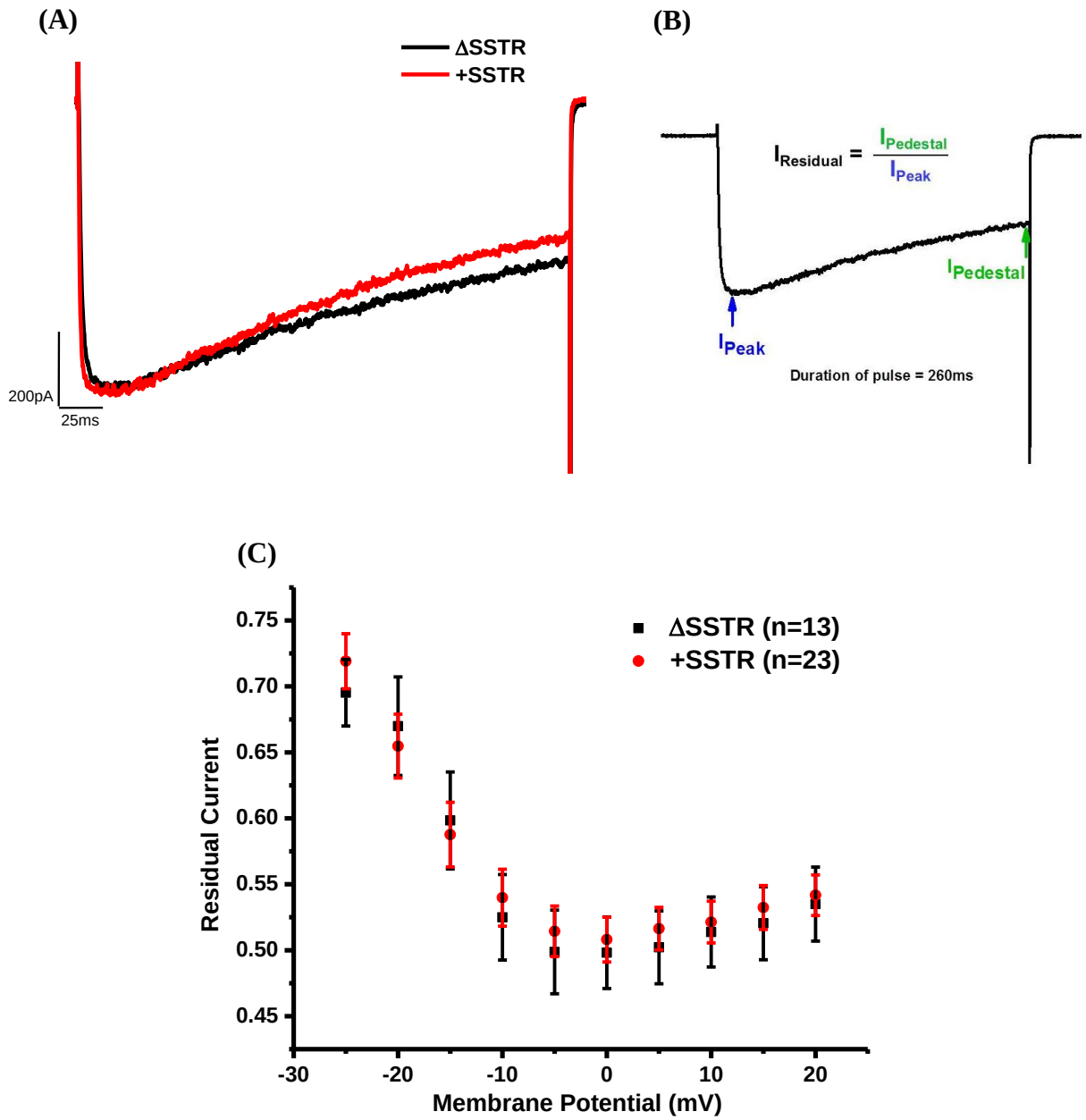

Figure 3.4: SSTR does not affect the degree of $Ca_v2.1$ inactivation
(A) Overlapped representative peak barium current traces from the IV protocol for the ΔSSTR (black) and +SSTR (red) splice variants showing the slow inactivation of current in barium-containing external solution. **(B)** Residual current ($I_{Residual}$) was calculated by dividing the current remaining at the end of a test pulse ($I_{Pedestal}$) by the peak current of the same test pulse (I_{Peak}). **(C)** Residual current for each splice variant was plotted against membrane potential and shows no significant difference in the amount of inactivation between the two splice variants.

3.3.4 The SSTR insertion affects voltage-dependence of $Ca_v2.1$ inactivation

The steady-state inactivation protocol consisted of a series of 500 ms conditioning pre-pulses ranging from -120 mV to +10 mV in 10 mV increments followed by an 80 ms test pulse to 0 mV (Figure 3.5A). Figures 3.5B and 3.5C show representative current traces elicited from the 80 ms test pulse to 0 mV which follow the conditioning pre-pulse for the ΔSSTR and +SSTR $Ca_v2.1$ splice variants, respectively. The peak current from each trace was plotted as a function of the pre-pulse potential and was fit with the Boltzmann equation (Figure 3.6A). I found a 5.04 mV difference in the membrane potential where half of the channels are inactivated ($V_{50inact}$) with the +SSTR splice variant having a more hyperpolarized $V_{50inact}$ than ΔSSTR ($V_{50inact}$ in mV = -47.13 ± 1.26 and -42.09 ± 1.55, respectively). There was no significant difference in the Boltzmann slope factor (k_{inact}) between the +SSTR and ΔSSTR variants (k_{inact}= 6.09 ± 0.15 and 6.18 ± 0.13, respectively).

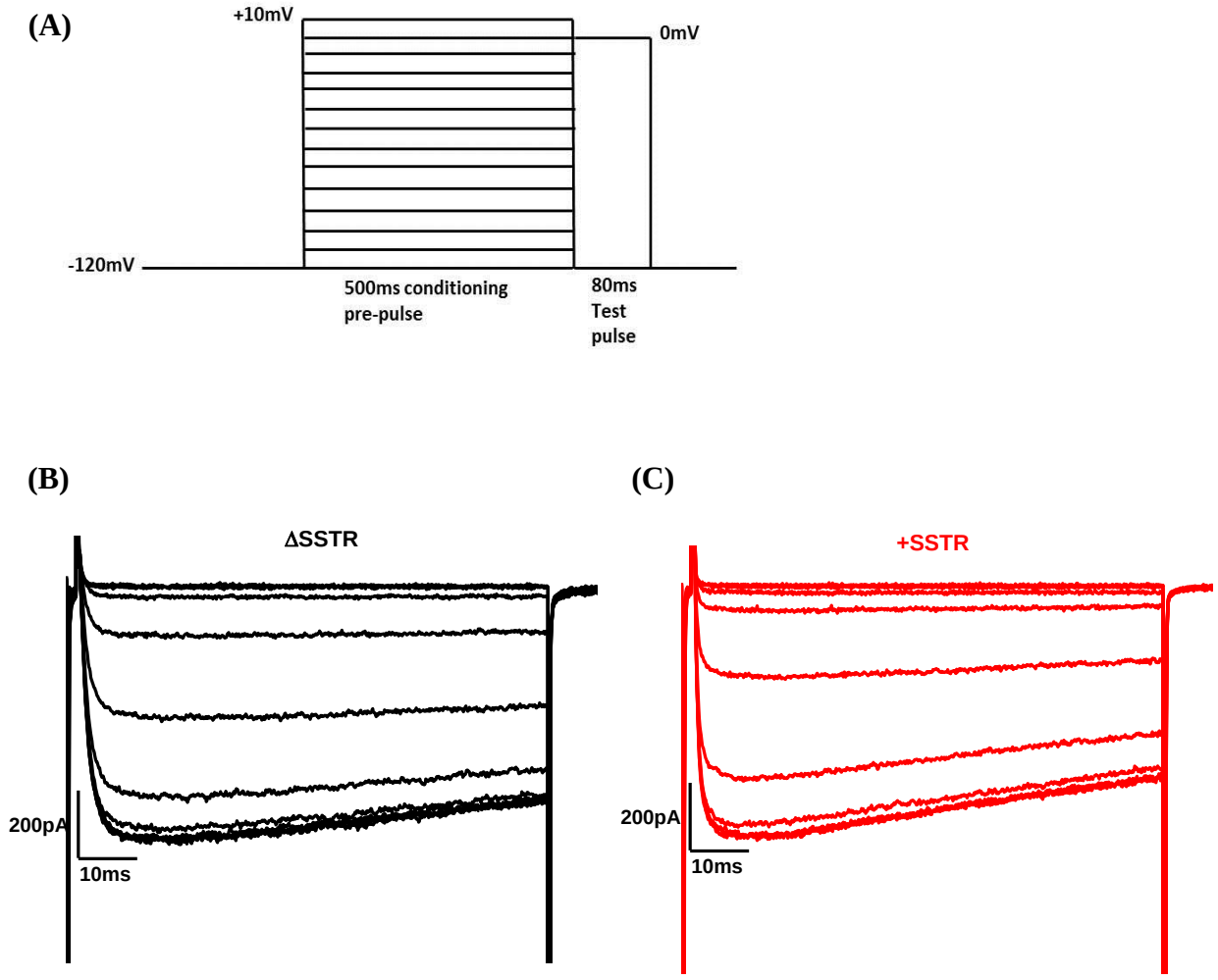

Figure 3.5: Barium currents evoked by the steady-state inactivation protocol to study the voltage-dependence of inactivation

Barium currents were evoked using a steady-state inactivation protocol in order to study the voltage-dependence of inactivation of the two splice variants. **(A)** Steady-state inactivation protocol consisting of a 500 ms conditioning pre-pulse at membrane potentials ranging from -120 mV to +10 mv in 10 mV increments followed by an 80 ms test-pulse to 0 mV. **(B)** and **(C)** Representative cells showing the barium currents evoked by the 80 ms test-pulse following the conditioning pre-pulse for ΔSSTR and +SSTR $Ca_v2.1$ channels, respectively.

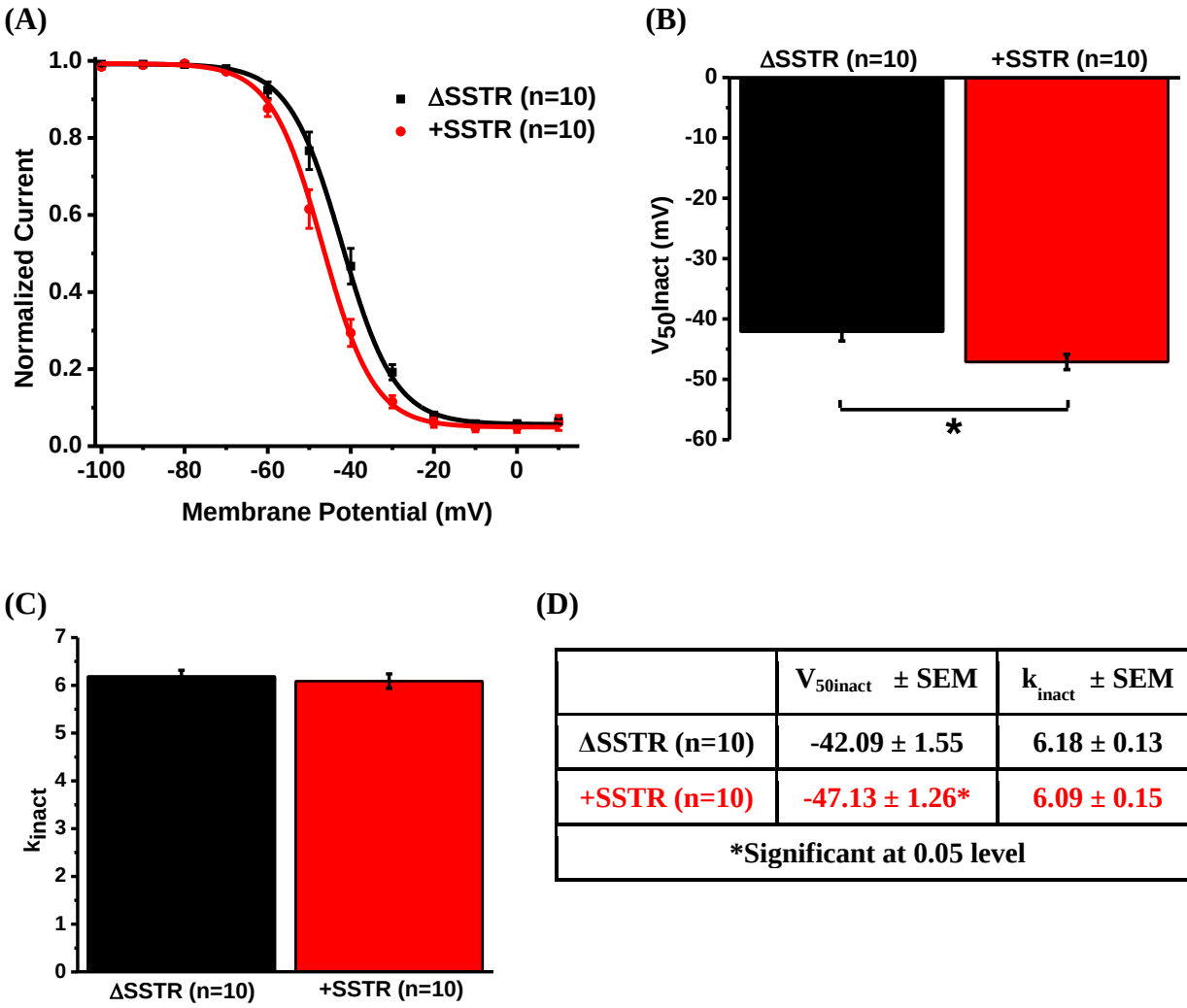

	$V_{50inact}$ ± SEM	k_{inact} ± SEM
ΔSSTR (n=10)	-42.09 ± 1.55	6.18 ± 0.13
+SSTR (n=10)	-47.13 ± 1.26*	6.09 ± 0.15
*Significant at 0.05 level		

Figure 3.6: SSTR affects the voltage-dependence of inactivation of $Ca_v2.1$
(A) Steady-state inactivation curve for ΔSSTR (black) and +SSTR (red) $Ca_v2.1$ splice variants generated by plotting the normalized peak current values as a function of the conditioning pre-pulse membrane potential. Steady-state inactivation curves were fit with the Boltzmann equation. **(B)** Bar graph showing mean $V_{50inact}$ (±SEM) with the +SSTR variant having a more hyperpolarized $V_{50inact}$ than ΔSSTR. **(C)** Bar graph showing mean k_{inact} (±SEM) with no significant difference between the ΔSSTR and +SSTR splice variants. **(D)** Table showing mean $V_{50inact}$ and k_{inact} values (±SEM). *p<0.05 (one-way ANOVA).

3.3.5 The ΔSSTR and +SSTR $Ca_v2.1$ splice variants respond differently to APW broadening

Due to the distinct activation kinetics and voltage-dependent properties of the splice variants, we wanted to determine whether these differences could affect the responses of the channels to APWs of different durations. I measured barium currents elicited by APWs with half-durations of 0.60 ms, 1.5 ms and 3.5 ms. Figure 3.7A shows the different APWs used (top graph) and representative current traces for the ΔSSTR (middle graph) and +SSTR (bottom graph) variants elicited by each APW. I found that the peak current amplitude for the ΔSSTR variant increased with increasing APW duration whereas the +SSTR variant showed decreasing peak current amplitude with increasing APW duration. Charge transference was measured by integrating the area under the current trace. While the charge transference through both variants increased with increasing APW duration, the rate of increase in charge transference was much greater for ΔSSTR channels than +SSTR containing channels with slopes of 0.47 ± 0.006 and 0.22 ± 0.03, respectively (Figure 3.7B and 3.7C).

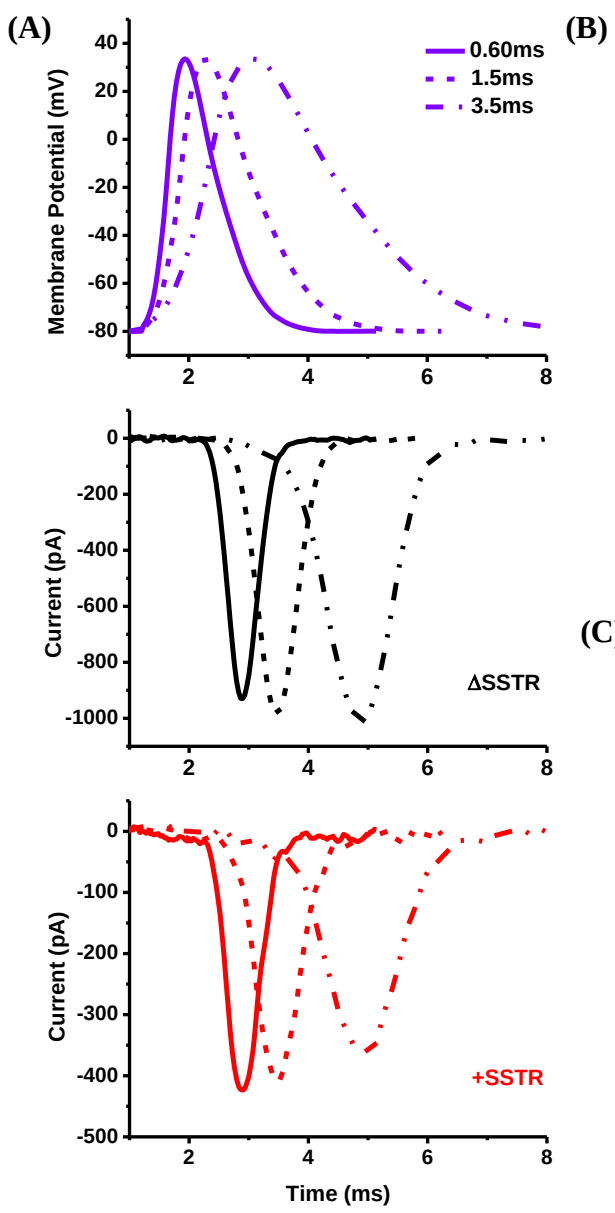

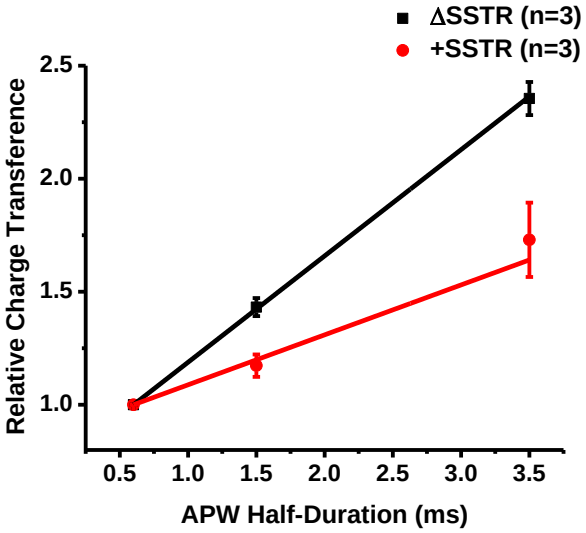

(C)

Relative increase in charge transfer		
	Action Potential Half-Duration	
	1.5ms	3.5ms
ΔSSTR (n=3)	1.43 ± 0.04	2.35 ± 0.07
+SSTR (n=3)	1.17 ± 0.05*	1.73 ± 0.16*
*Significant at 0.05 level		

Figure 3.7: The ΔSSTR and +SSTR $Ca_v2.1$ splice variants respond differently to APW broadening

(A) The top graph shows the three APW commands with half-durations of 0.6 ms, 1.5 ms and 3.5 ms that were used to elicit barium currents. The middle and bottom graphs show representative traces of currents elicited from the different APWs for the ΔSSTR and +SSTR channels, respectively. **(B)** Line graph showing the relative increase in charge transference (±SEM) with increasing APW duration relative to the shortest APW duration (0.6 ms). Charge transference through ΔSSTR channels (in black) is more sensitive to increasing APW duration than +SSTR channels (in red). **(C)** Table showing the mean values (±SEM) of the relative increase in charge transference with increasing APW duration. *p<0.05 (one-way ANOVA).

3.4 Discussion

In comparing the properties of macroscopic barium currents between the $Ca_v2.1$ ΔSSTR and +SSTR splice variants I found that channels possessing +SSTR have faster activation kinetics and more hyperpolarized V_{50act} and $V_{50inact}$ values. These findings suggest that SSTR insertion in the S3-S4 linker of domain III affects the gating of the $Ca_v2.1$ channel, perhaps due to its close proximity to the S4 voltage sensor which moves upon membrane depolarization driving the channel to activate (Bezanilla, 2000; Bezanilla, 2002; Catterall *et al.*, 2007; Catterall, 2010)

Activation and deactivation kinetics of VGCCs are strongly voltage-dependent and as a result calcium influx evoked by an action potential (AP) can have a great dependence on the duration and shape of the AP (Bean, 2007). Differences in the response to APs are especially important at presynaptic terminals, where $Ca_v2.1$ channels are heavily concentrated, and modest changes in APWs can result in significant changes in calcium entry and subsequently the strength and timing of neurotransmitter release (Sabatini and Regehr, 1999; Bean, 2007). As such, it was of interest and relevance to determine whether the differences in the biophysical properties, especially the activation kinetics, between the splice variants could alter channel responses to APWs with varying durations.

I compared the currents elicited by the different APWs and found that the ΔSSTR and +SSTR variants show a difference in their responses to increasing APW durations. For ΔSSTR-containing channels, increasing the APW duration led to an increase in the peak current amplitude, most likely resulting from greater recruitment of activated channels during a longer rising phase before the driving force is increased at the repolarization phase. In contrast, the faster activating +SSTR-containing channels showed decreasing peak current amplitudes with

increasing APW duration, most likely because their maximum activation occurs with the shortest APW duration as they activate faster followed by partial deactivation once the driving force is finally increased (Geiger and Jonas, 2000).

The integral of the current is a more accurate predictor of neurotransmission initiation than the peak current amplitude and corresponds to the charge transference through the channel (Borst and Sakmann, 1999). In calculating the charge transference, I found that although both variants showed the expected increase in charge transference due to increasing APW duration, entry through ΔSSTR splice variant channels was significantly more sensitive to changes in APW duration and had a steeper slope for charge transference increase than +SSTR variant channels. These differences suggest that each channel variant could have specific roles in processing different types of AP-mediated information. The lesser sensitivity of charge transference through +SSTR $Ca_v2.1$ channels with changes in APW would allow these channels to be more reliable reporters of action potential frequency whereas ΔSSTR $Ca_v2.1$ channels due to their sensitivity to different APW durations would allow more variation in the amount of neurotransmitter release resulting from different types of AP stimuli (McCobb and Beam, 1991; Sabatini and Regehr, 1999).

Together, the results from this study show that alternative splicing in a key functional region of $Ca_v2.1$ channels produces significant changes in biophysical properties which can translate into variations in the response of the channel to different AP stimuli. This diversity in functional activity should help us define the specific roles that splice variants play in the processing of synaptic information and further aid in our understanding of mechanisms that contribute to the complexity and efficiency of CNS physiological processes.

Chapter 4: Effects of SSTR Insertion on the Sensitivity of $Ca_V2.1$ Channels to ω-Agatoxin-IVA

4.1 Introduction

The peptide toxin ω-Agatoxin-IVA inhibits $Ca_v2.1$ channels by altering the voltage-dependence of gating of the channel (Mintz *et al.,* 1992b; McDonough *et al.,* 1997b). In binding to the S3-S4 extracellular linker of domain IV ω-Aga-IVA is thought to "trap" the voltage sensor that normally moves outward upon depolarization in its inward resting position thereby preventing the channel from undergoing a conformational change required to activate (McDonough, 2007; Catterall *et al.,* 2007). As a result, moderate depolarizations that normally activate the channel are too weak and more energy is needed in order for the channels to activate. Studies have shown that insertion of NP in the S3-S4 linker of domain IV can alone cause a 10-fold decrease in $Ca_v2.1$ sensitivity to ω-Aga-IVA by sterically hindering or weakening the toxin's binding site (Hans *et al.,*1999b; Bourinet *et al.,* 1999; Winterfield and Swartz, 2000; McDonough 2007). However, it has been suggested that the other three channel domains could also play a role in the mechanism of action of current inhibition since the voltage sensors of all four domains need to move in order for the channel to activate (Winterfield and Swartz, 2000; McDonough 2007).

The SSTR insertion in the S3-S4 linker of domain III is in a homologous region as the NP insertion in the S3-S4 linker of domain IV and we hypothesized that the SSTR insertion may also affect the sensitivity of $Ca_v2.1$ channels to ω-Aga-IVA. Using whole-cell patch-clamp electrophysiology, I compared the effects of 10 nM ω-Aga-IVA on ΔSSTR and +SSTR $Ca_v2.1$

channels. I found that there was no significant difference in current block due to ω-Aga-IVA between the splice variants suggesting that SSTR insertion does not alter $Ca_v2.1$ channel sensitivity to ω-Aga-IVA and most likely does not disrupt the binding site of the toxin.

Knowledge of the pharmacological properties of $Ca_v2.1$ isoforms is important as ω-Aga-IVA is commonly used to block $Ca_v2.1$ channels in studies conducted on primary neurons that express a variety of VGCCs. Additionally, the mechanism of action of ω-Aga-IVA on $Ca_v2.1$ channel activity can be mimicked in order to develop therapeutic drugs for diseases in which gain-of-function effects due to $Ca_v2.1$ channel mutations are observed.

4.2 Methods

4.2.1 ω-Agatoxin-IVA solutions

Bovine serum albumin (BSA) (Sigma-Aldrich ; Cat: A-2153, Lot 29H0946) was added to the 5 mM barium external solution (see Chapter 3 methods) at a concentration of 0.25mg/mL in order to prevent nonspecific binding of the toxin to the perfusion tubing and testing chamber. Recombinant ω-Agatoxin-IVA (Alomone Labs; Cat: STA-500, Lot: STA500TX0401) was reconstituted in H_2O and 50 uM stock aliquots were stored at -20^oC and thawed immediately before use and were not refrozen. The working concentration of 10 nM ω-Aga-IVA in BSA-containing 5 mM barium external solution was made and added to the perfusion tube immediately before it was perfused into the testing chamber at a speed of 1.5mL/minute.

4.2.2 Time course protocol and data analysis

Peak barium current was elicited by a 30 ms test pulse to 0 mV from a holding potential of -90 mV and was delivered every seven seconds. Prior to the 0 mV test pulse, the time course protocol also contained a 5 ms step pulse to -85 mV in order to monitor potential changes in

series resistance throughout testing to rule out the possibility that decrease in current amplitude was a result of increase in series resistance (Figure 4.1A). The peak current value from each trace was plotted as a function of time to generate a time course of current inhibition. The percentage of remaining current was calculated by dividing the remaining current value at the end of toxin application by the peak current value prior to toxin application. The time constant for the development of current block was determined by fitting the portion of the time course during which the effect of the toxin is seen (Figure 4.4A) with a single exponential function, $I=Ae^{-t/\tau}$, where A is the current amplitude and τ is the time constant.

Because rundown of current amplitude was seen as a result of continuous stimulation during testing, the current decay due to rundown was compared to current inhibition by ω-Aga-IVA. The amount of current decrease in Figure 4.5 was determined at the 30 minute mark as this was a time point where the most number of cells that were studied reached during testing. Rundown between the splice variants was also compared in order to make sure that it was not significantly different between the splice variants. The slope of the rundown of current amplitude was determined by fitting the time course with a linear function, $I=I_{max} + mt$, where I_{max} is the maximum normalized current at rundown initiation, I is the normalized current, t is time (in minutes) and m is the slope (corresponding to the percentage of current decay per minute).

4.3 Results

4.3.1 NP insertion decreases sensitivity of $Ca_v2.1$ to ω-Agatoxin-IVA

In order to validate the experimental set-up I first tested and compared the sensitivities of the +NP and –NP splice variants of $Ca_v2.1$ to ω-Aga-IVA. Barium currents were elicited every

seven seconds by a 30 ms test pulse to 0 mV from a holding potential of -90 mV. Figures 4.1B and 4.1C show every seventh current trace elicited (equivalent to every 49 seconds) during the recording process in order to show the progression of current inhibition following 10 nM ω-Aga-IVA application at the 2 minute and 20 seconds mark for -NP and +NP, respectively. The peak current from each trace was plotted as a function of time in order to generate the representative time courses seen in Figure 4.1D. The bar graph in figure 4.1E shows the averaged percentage of current remaining following toxin application. I found a significant difference in the amount of current remaining following application of 10 nM ω-Aga-IVA between the -NP and +NP splice variants with the +NP variant showing a much smaller decrease in current amplitude (remaining current % = 9.44 ± 1.44 and 44.98 ± 7.23, respectively). Therefore, in agreement with previous reports, I have shown that NP insertion significantly decreases the sensitivity of $Ca_v2.1$ channels to ω-Aga-IVA (Bourinet *et al.,* 1999)**.**

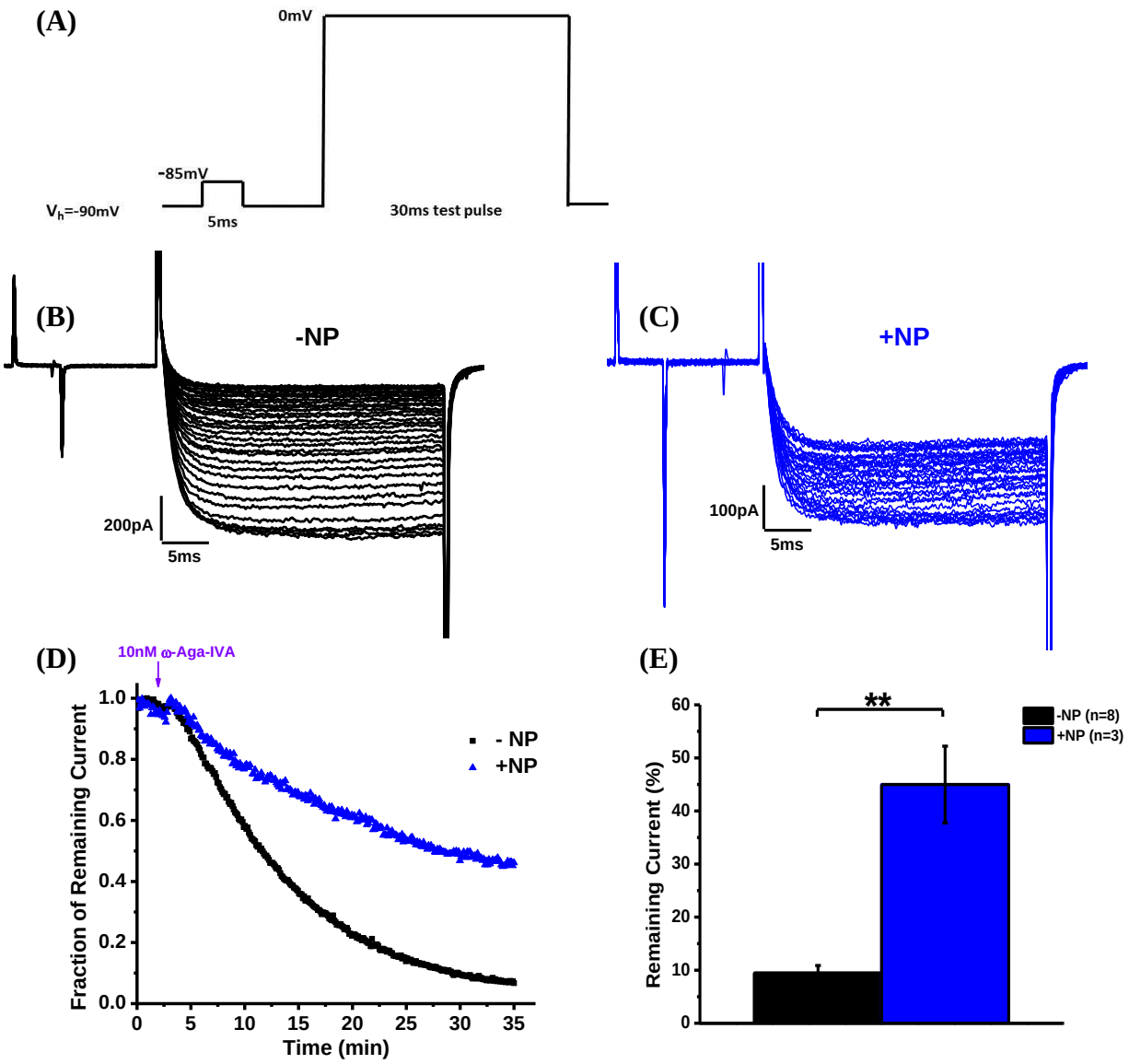

Figure 4.1: NP insertion significantly decreases the sensitivity of $Ca_v2.1$ to ω-Agatoxin-IVA
(A) Protocol used to evoke continuous peak current stimulation during toxin application. Protocol consisted of a 5 ms depolarizing pulse to -85 mV from a holding potential of -90 mV to monitor any changes in series resistance followed by a 30 ms test pulse to 0 mV in order to evoke peak current amplitude. Pulses were applied every seven seconds. **(B)** and **(C)** Representative traces of every seventh test pulse elicited (i.e. every 49 seconds) to show progression of current inhibition following application of 10 nM ω-Aga-IVA for the –NP and +NP splice variants, respectively. **(D)** Representative time courses of current inhibition of the –NP (black squares) and +NP (blue triangles) splice variants following application of 10 nM ω-Aga-IVA generated by plotting normalized peak current value from each test pulse as a function of time. **(E)** Bar graph showing the average percentage of current remaining following application of 10 nM ω-Aga-IVA calculated by dividing the remaining current at the end of toxin application by the peak current value before toxin application. **p<0.01 (one-way ANOVA).

4.3.2 SSTR insertion does not affect current block by ω-Agatoxin-IVA

Figures 4.2A and 4.2B show the barium currents elicited by every seventh test pulse (equivalent to every 49 seconds) during the recording process in order to show the progression of current inhibition following 10 nM ω-Aga-IVA application at the 2 minute and 20 seconds mark for ΔSSTR and +SSTR, respectively. Figure 4.2C displays representative time courses for each splice variant with ΔSSTR in black and +SSTR in red. In measuring the percentage of remaining current (dividing the remaining current by the peak current prior to ω-Aga-IVA application) I found no significant difference in the degree of current block seen with application of 10 nM ω-Aga-IVA between the ΔSSTR and +SSTR variants (remaining current % = 9.44 ± 1.44 and 11.85 ± 1.53, respectively) (Figure 4.2D). Figures 4.2E and 4.2F show representative IV curves of each splice variant before (filled in symbols) and after (checked symbols) 10 nM ω-Aga-IVA application to show the extent of current block.

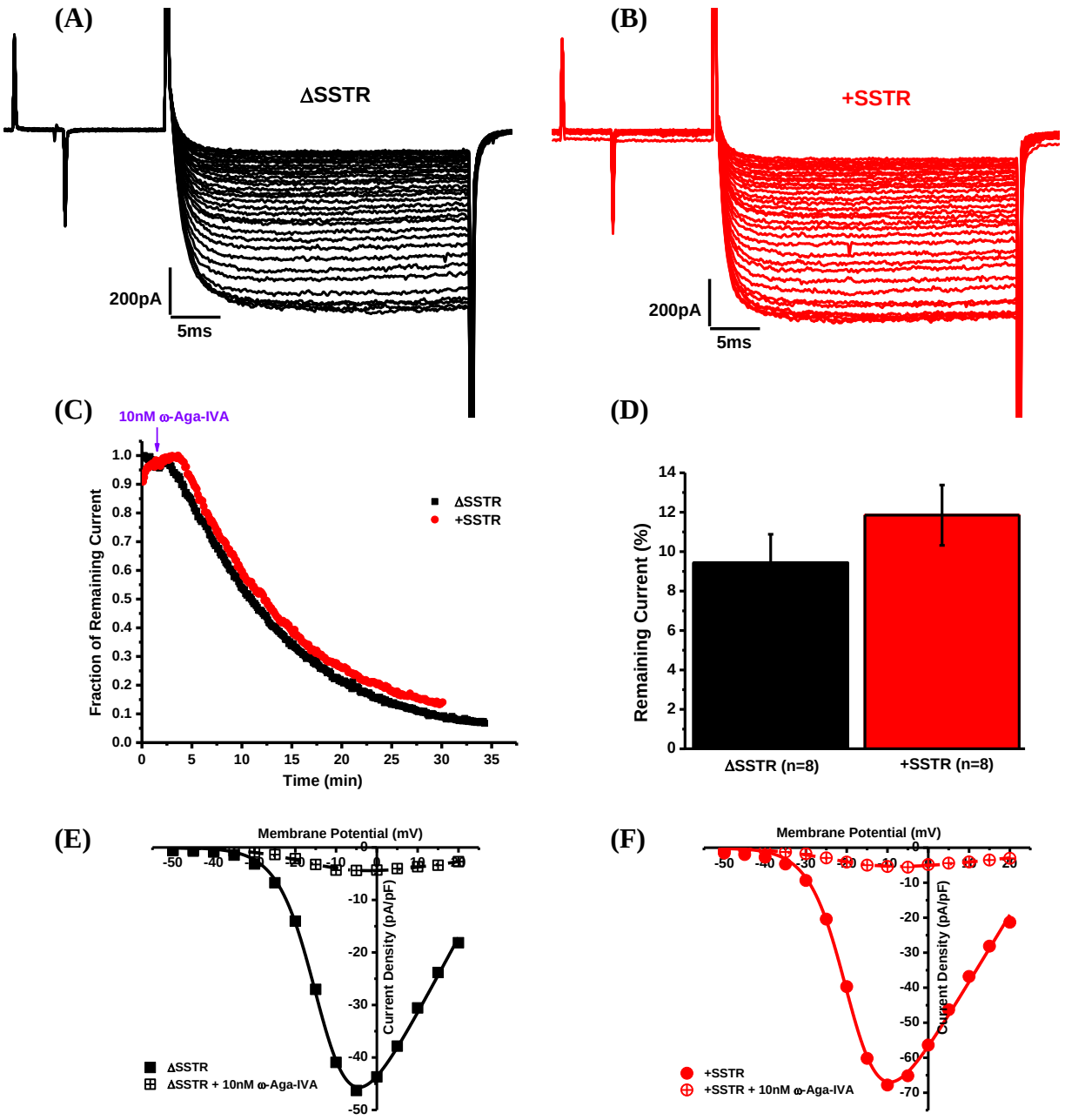

Figure 4.2: SSTR insertion does not affect current block by 10 nM ω-Agatoxin-IVA
(A) and **(B)** Representative traces of every seventh test pulse elicited (i.e. every 49 seconds) to show progression of current inhibition following application of 10 nM ω-Aga-IVA for the ΔSSTR and +SSTR splice variants, respectively. **(C)** Representative time courses of current inhibition during toxin application for the ΔSSTR variant (black squares) and +SSTR variant (red circles) generated by plotting peak current from each test pulse as a function of time. **(D)** Bar graph showing percentage of current remaining following toxin application. **(E)** and **(F)** Representative IV curves before (solid symbol) and after (checkered symbol) toxin application showing the extent of current block for ΔSSTR and +SSTR, respectively.

4.3.3 SSTR insertion does not affect the time constant of development of block by ω-Agatoxin-IVA

I also wanted to determine whether there was any difference in the time constant of development of current block between the splice variants. Because the time course of current inhibition due to 10 nM ω-Agatoxin-IVA application followed a single exponential function I was able to fit the time course and obtain the time constant. Only the portion of the time course that exhibited an effect of the toxin was fit with the single exponential function (see Figure 4.3A). I found no significant difference in the time constant of development of current block between the ΔSSTR and +SSTR splice variants (τ_{on} in minutes = 11.15 ±1.46 and 10.22 ± 0.81, respectively).

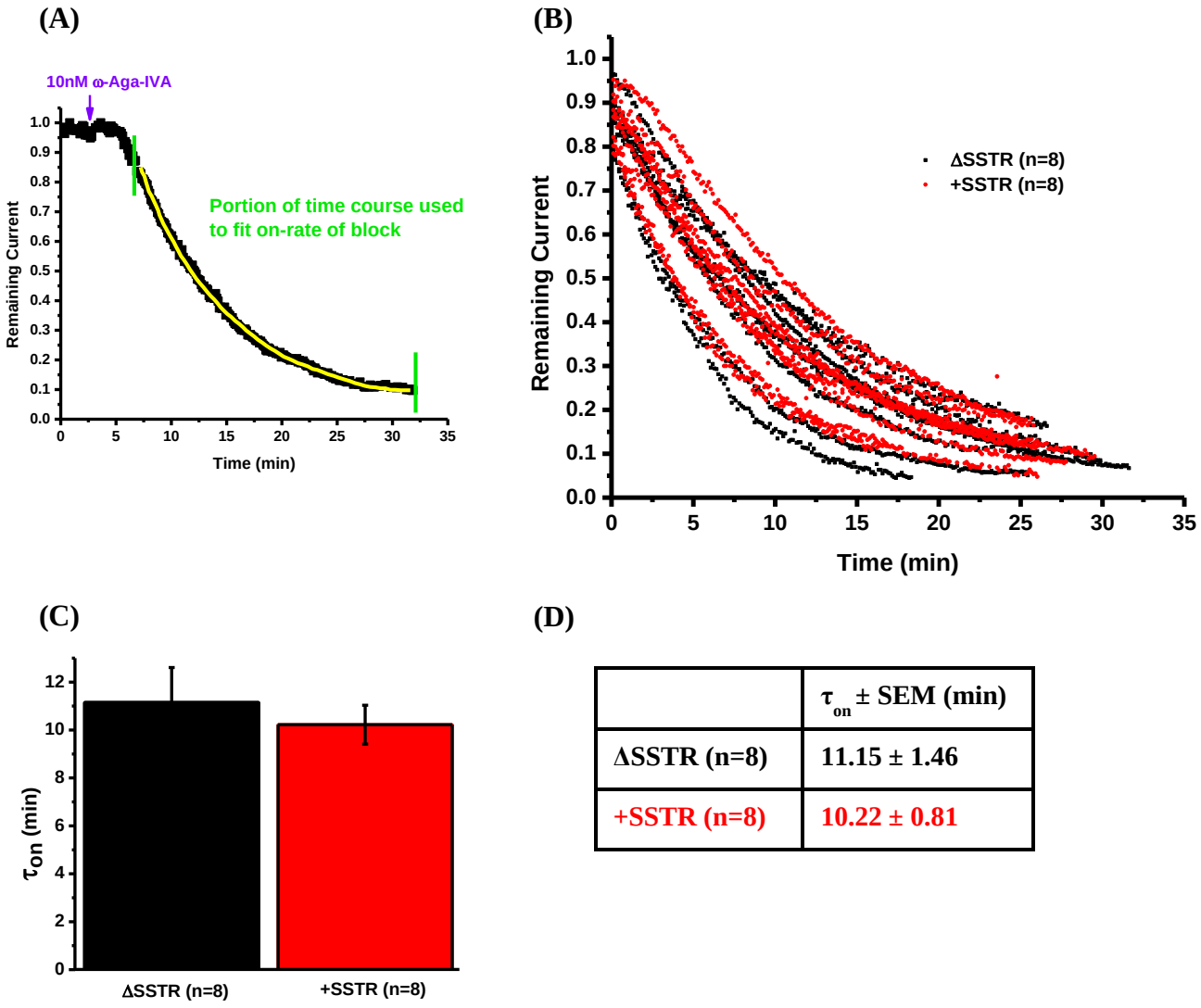

	τ_{on} ± SEM (min)
ΔSSTR (n=8)	11.15 ± 1.46
+SSTR (n=8)	10.22 ± 0.81

Figure 4.3: SSTR insertion does not affect the time constant of development of current block due to 10 nM ω-Agatoxin-IVA

(A) Example of fitting of time course (shown in yellow) with a single exponential function to obtain the time constant (τ_{on}). Only the portion of the time course exhibiting an effect of the toxin (between the green bars) was fit. **(B)** Portion of time courses used for fittings to get the time constant showing that although there is variability between different cells, there is no significant difference between the ΔSSTR (in black) and +SSTR (in red) splice variant-expressing cells. **(C)** Bar graph displaying mean values for time constants of development of current block with no significant differences between the two splice variants. **(D)** Table showing mean values (±SEM) of time constant of development of current block.

4.3.4 The decrease in current amplitude is not solely due to rundown

Rundown of HVA current amplitude is often seen during whole-cell patch-clamp experiments with continuous stimulation due to depletion of the plasma membrane phospholipid PIP_2 (Wu *et al.,* 2002; Suh *et al.,* 2010). Although Mg-ATP, shown to prevent rundown of current amplitude, was added to the internal solution I still observed a decrease in current amplitude during continuous stimulation over extended periods of testing (Wu *et al.,* 2002; Suh *et al.,* 2010). Therefore in order to confirm that the decrease in current amplitude seen during toxin application was not a reflection solely due to rundown I performed control experiments by perfusing external solution containing only BSA onto cells under the same experimental conditions as before including the rate of perfusion and duration of stimulation. I found that for both splice variants there was a significant difference in the amount of total current decrease with or without toxin application following a 30 minute testing procedure signifying that rundown was not the main source of current decay during toxin application (Figure 4.4C and D). Additionally, figures 4.4A and 4.4B show that the time course of current decay due to rundown follows a linear path whereas current inhibition due to toxin application follows a single exponential function.

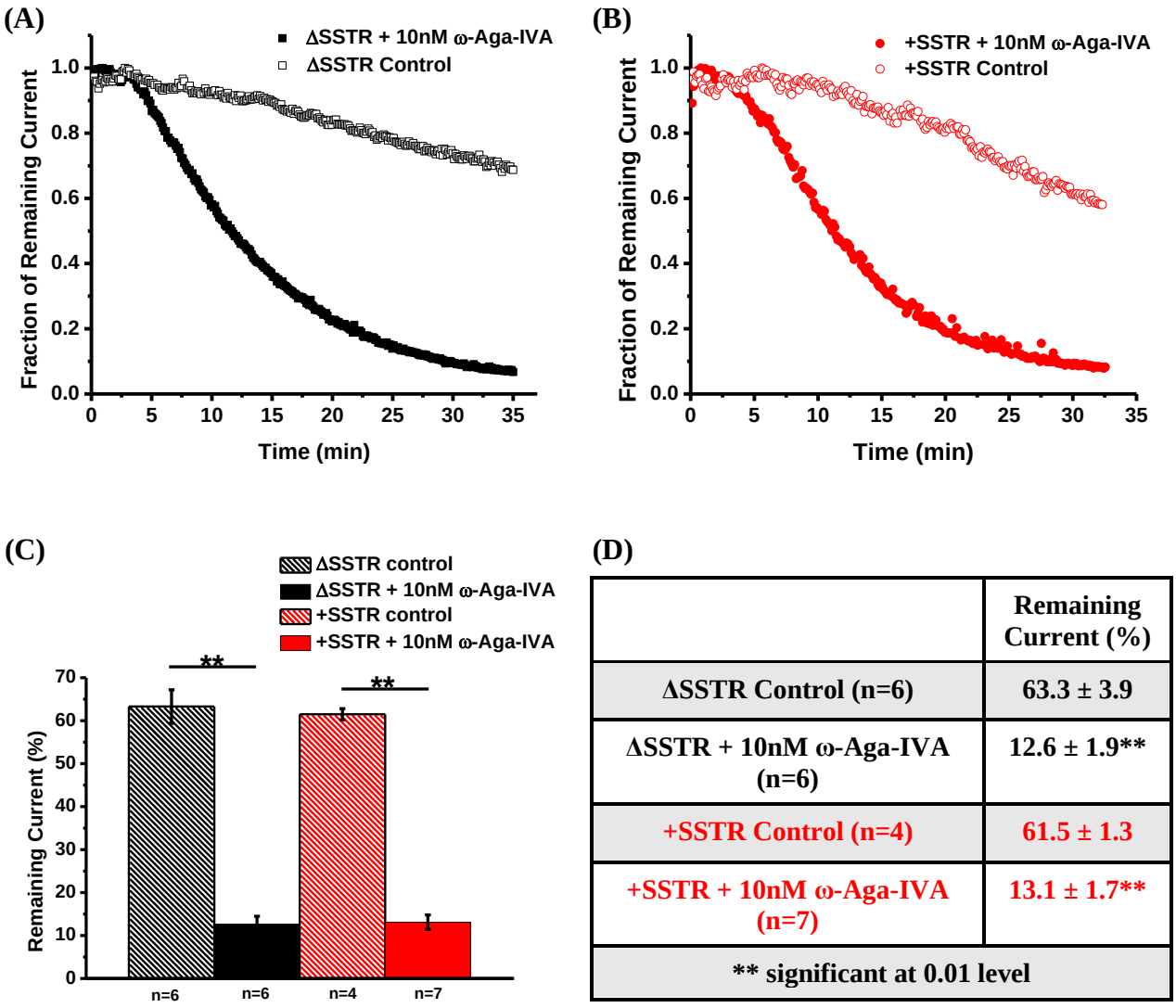

(D)

	Remaining Current (%)
ΔSSTR Control (n=6)	63.3 ± 3.9
ΔSSTR + 10nM ω-Aga-IVA (n=6)	12.6 ± 1.9**
+SSTR Control (n=4)	61.5 ± 1.3
+SSTR + 10nM ω-Aga-IVA (n=7)	13.1 ± 1.7**
** significant at 0.01 level	

Figure 4.4: Decrease in current amplitude following ω-Agatoxin-IVA application is not solely due to current rundown during continuous stimulation

Rundown of current amplitude is often seen during continuous stimulation of HVA channels in whole-cell patch-clamp electrophysiology experiments. This figure verifies that the current inhibition seen in previous figures due to ω-Aga-IVA application is not solely due to rundown but is mainly a result of the effects of the toxin. **(A)** and **(B)** Representative time courses for ΔSSTR and +SSTR with (filled symbols) or without (open symbols) 10 nM ω-Aga-IVA application demonstrating that current decay due to ω-Aga-IVA application follows a single exponential function whereas current decay due to rundown is linear. **(C)** Bar graph displaying the percentage of current remaining following 30 minutes of testing with or without toxin application showing that for both splice variants there is a clear distinction between the amount of current inhibition with or without toxin application. **(D)** Table showing the values of the amount of current remaining. **$p < 0.01$ (one-way ANOVA).

4.3.5 Rundown between the ΔSSTR and +SSTR $Ca_v2.1$ splice variants is not significantly different

It was also important to demonstrate that there was no significant difference between the rundown of the splice variants which could potentially influence the toxin application results. Firstly, I fit the rundown time course of each cell with a linear function in order to obtain the slope of the rundown which corresponds to the percentage of current decay per minute (Figures 4.5A and B). I found that there was no significant difference in the slope of run down between the ΔSSTR and +SSTR splice variants (% current decay/minute = -1.32 ± 0.15 and -1.48 ± 0.05, respectively). Secondly, in comparing the amount of current decay following 30 minute testing by dividing the remaining current by the peak current before the testing duration I found that there was no significant difference in the amount of current remaining between the splice variants (% of current remaining = 56.0 ± 4.0 and 52.8 ± 2.2). Because I did not find significant differences in the rundown characteristics between the splice variants I did not have to adjust the values obtained from my ω-Aga-IVA studies.

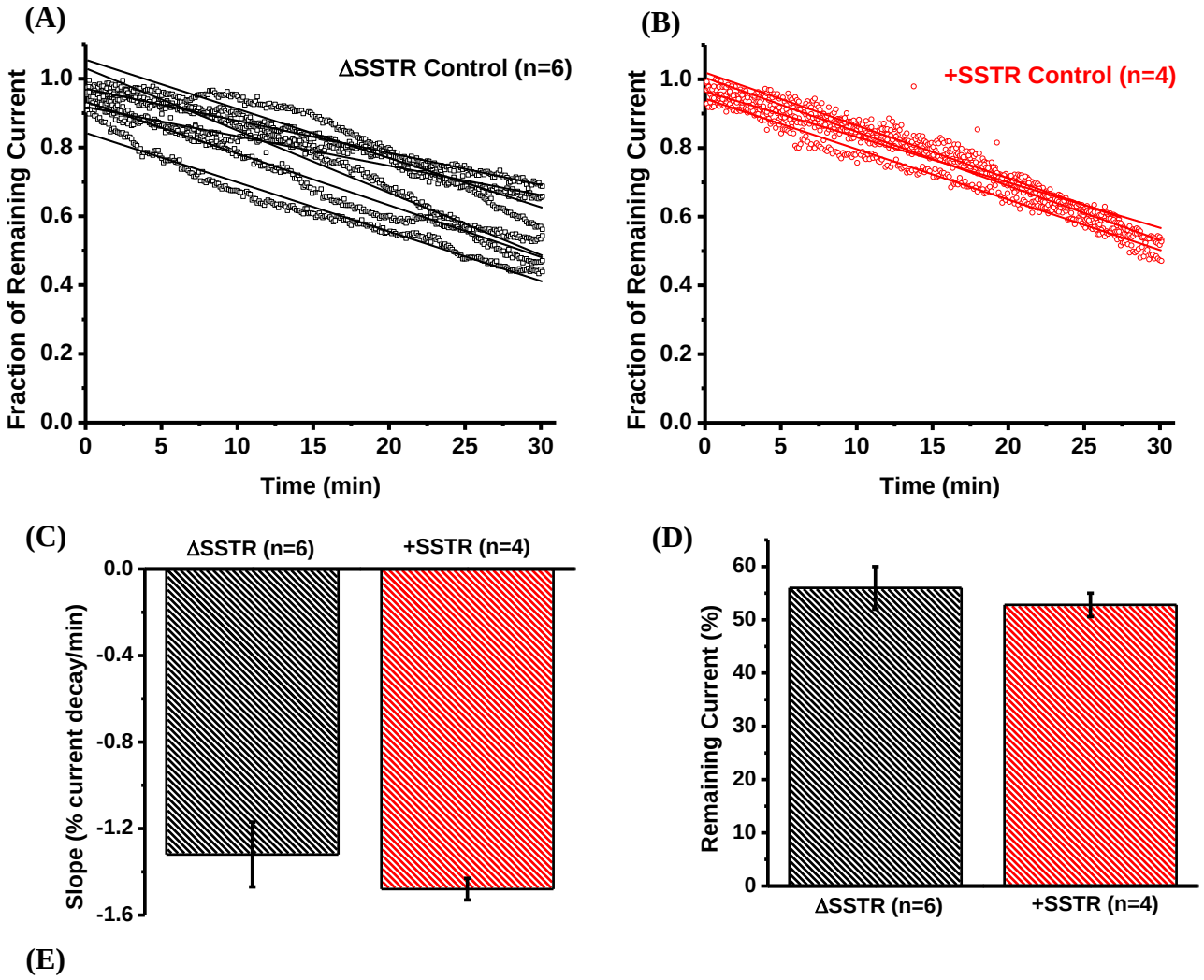

(E)

	Remaining current (%)	Slope (% current decay/min)
ΔSSTR (n=6)	56.0 ± 4.0	-1.32 ± 0.15
+SSTR (n=4)	52.8 ± 2.2	-1.48 ± 0.05

Figure 4.5: Rundown is not significantly different between the ΔSSTR and +SSTR $Ca_v2.1$ splice variants

(A) and **(B)** The portion of the time courses fit with a linear function in order to obtain the slope of rundown for ΔSSTR and +SSTR, respectively. **(C)** Bar graph comparing the slope of the rundown between the splice variants which represents the amount of current decay per minute. There was no significant difference in slope of the rundown between the two splice variants. **(D)** Bar graph showing percentage of current remaining after 30 minutes with no significant difference between the two splice variants. **(E)** Table showing mean values (±SEM) of slope of rundown and percentage of remaining current.

4.4 Discussion

The splice variant insertion of two amino acids, NP, in the S3-S4 extracellular linker of domain IV results in a significant decrease in the sensitivity of $Ca_v2.1$ channels to the peptide toxin ω-Aga-IVA (Bourinet *et al.,* 1999). The +SSTR splice variant has an insertion of four amino acids, SSTR, in the S3-S4 extracellular linker of domain III bringing into question whether it too could affect $Ca_v2.1$ sensitivity to ω-Aga-IVA. However, I found that the insertion of +SSTR does not have a significant effect on the sensitivity of $Ca_v2.1$ channels to ω-Aga-IVA as there were no significant differences in the amount of current block by 10 nM ω-Aga-IVA nor was there a significant difference in the time constant of development of block. These results suggest that unlike +NP insertion in domain IV, +SSTR insertion in domain III does not disrupt the binding site for ω-Aga-IVA. As a result, +SSTR-containing channels are targets for ω-Aga-IVA blockade *in vivo* and *in vitro*. Further, +SSTR-containing channels would be targets for therapeutic drugs developed based on the functional properties of ω-Aga-IVA to treat $Ca_v2.1$ gain-of-function disorders.

Chapter 5: Discussion

5.1 Main findings

The +SSTR splice variant, consisting of a four amino acid insertion in the S3-S4 extracellular linker of domain III, is estimated to be included in approximately 10% and 24% of $Ca_v2.1$ transcripts in whole mouse brain and rat brain, respectively (Allen *et al.*, 2010; Snutch Lab unpublished data). Prior to this study, detailed analysis of its spatial expression profile in the rodent CNS as well as effects on the biophysical and pharmacological properties of $Ca_v2.1$ channels had not yet been reported. The main goal of this thesis was to begin the characterization of the +SSTR splice variant in order to help uncover its distinct functional properties and potential impact on CNS physiology. My hypothesis was that the +SSTR splice variant channels would be differentially expressed throughout the CNS and also that the SSTR insertion could potentially impact distinct biophysical and pharmacological properties compared to the more prevalent ΔSSTR-variant channels.

My first objective was to generate an expression profile of the +SSTR splice variant by analyzing expression levels in different regions of the rat CNS. Performing splice variant-specific quantitative real-time PCR on ten different regions of the adult Sprague Dawley rat CNS, I found that in contrast to the overall abundance observed for whole brain RNA, there are three specific regions of the CNS wherein +SSTR-variant channels are significantly more abundant than ΔSSTR-variant channels. These regions are the brainstem, reticular thalamus and spinal cord. The widely expressed splicing factor Nova-2 has been shown to enhance SSTR insertion and could be more active or more abundantly expressed in these regions (Allen *et al.*,

2010). Alternatively, additional splicing factors may also affect +SSTR splicing and could collectively be causing the differential expression of the +SSTR variant throughout the CNS.

A second objective was to determine the effects of SSTR insertion on the biophysical properties of $Ca_v2.1$ as the SSTR insertion is in close proximity to the S4 voltage sensor that has to move following depolarization in order for the channel to activate (Bezanilla, 2000; Catterall *et al.,* 2007; Catterall, 2010). Using whole-cell patch-clamp electrophysiology I found that the +SSTR splice variant channels exhibit faster activation kinetics and more hyperpolarized V_{50act} and $V_{50inact}$ values than the ΔSSTR variant channels. Further, to study the effects of these differences in biophysical properties on the response of the channel to more physiological depolarizations, I tested the response of the two splice variants to APWs with different durations. I found that although both variants exhibited an increase in charge transference with APW broadening, the +SSTR variant showed less sensitivity to APW duration than the ΔSSTR variant. The differences in sensitivity between the splice variants to APW broadening may underlie distinct roles these two variants play in transmitting different types of action potential-encoded information. It has been suggested that insensitivity of charge transference to APW broadening, such as is seen for the +SSTR variant, results in greater accuracy of action potential frequency whereas sensitivity to APW duration allows for more variation in the amount of neurotransmitter release in response to different types of APWs (McCobb and Beam, 1991).

My third objective was to determine the potential effects of SSTR insertion on the sensitivity of $Ca_v2.1$ to the gating modifier peptide toxin ω-Aga-IVA. It has been established previously that the insertion of NP in the S3-S4 extracellular linker of domain IV causes a significant decrease in the sensitivity of $Ca_v2.1$ to ω-Aga-IVA (Bourinet *et al.,* 1999). However, as it has been suggested that the other three domains of the channel could also be involved in the

mechanism of current inhibition by the toxin we wanted to test whether SSTR insertion in the S3-S4 extracellular linker of domain III might also affect the sensitivity of $Ca_v2.1$ to ω-Aga-IVA (Winterfield and Swartz, 2000). I found that with 10 nM ω-Aga-IVA there were no significant differences in the current inhibition between the +SSTR and ΔSSTR variants suggesting that SSTR insertion does not disrupt an ω-Aga-IVA binding site and does not affect the sensitivity of $Ca_v2.1$ to ω-Aga-IVA. Therefore, +SSTR-containing $Ca_v2.1$ channels are eligible targets for block by ω-Aga-IVA as well as potential therapeutic mimetics of the toxin.

5.2 Possible physiological relevance of findings

Findings from this thesis give further evidence that alternative splice variants of $Ca_v2.1$ are differentially expressed throughout the CNS and that alternative splicing in key functional regions of $Ca_v2.1$ can cause significant differences in biophysical properties. Additionally, I have shown that the differences in biophysical properties between splice variants can translate into distinct responses to different types of AP stimuli.

For the faster activating +SSTR variant $Ca_v2.1$ channels, I found that the charge transference was less sensitive to AP duration which may allow the channels to be better reporters of AP frequency which is essential for synapses that rely on precise timing (McCobb and Beam, 1991). For example, in the auditory pathway that connects the inner ear and brainstem, the synapse between the calyx of Held and soma of a medial nucleus of the trapezoid body neuron depends on precise timing for accurate sound localization (Sakmann, 2006). In fact, the results in Chapter 2 show that the +SSTR variant is predominantly expressed in the brainstem where it may play a role in facilitating various processes, such as sound localization, that depend on accurate timing of synaptic transmission (Figure 2.1A).

For ΔSSTR variant $Ca_v2.1$ channels I found that charge transference was more sensitive to AP duration thereby allowing more variation in the amount of response (McCobb and Beam, 1991). This capability can enhance synaptic strength as a result of increased calcium entry during AP broadening which, for example, can occur in an activity-dependent manner in hippocampal mossy fibers (McCobb and Beam, 1991; Wheeler *et al.,* 1996; Sabatani and Regehr, 1997; Geiger and Jonas, 2000; Zucker and Regehr, 2002). The studies in Chapter 2 have shown that the ΔSSTR variant channels are more abundantly expressed in the hippocampus where they may in fact help facilitate such occurrences (Figure 2.1A).

The findings from this thesis support the theory that alternative splicing provides fine-tuning of VGCC activity in order to fulfill the specific needs of different cell and tissue types or stimuli to effectively mediate synaptic transmission (Krovetz *et al.,* 2000; Liao *et al.,* 2009; Lipscombe *et al.,* 2013). As such, the combination of unique properties and specific ranges of expression of splice variants contributes to the complexity and efficiency of CNS synaptic signalling.

5.3 Potential limitations

The electrophysiology experiments using HEK 293 cells transfected with $Ca_v2.1$ cDNA provided a controlled environment that was ideal to study differences in functional properties between the +SSTR and ΔSSTR variants. This heterologous system however does not reflect an accurate representation of native channel populations in which a variety of different combinations of splice variants can be incorporated into each channel isoform and could have diverse impacts on the functional properties of the +SSTR and ΔSSTR variants. As such, full-length cDNA sequences of the entire population of expressed $Ca_v2.1$ channels would provide a

clearer picture of the predominance of certain splice variants along with their proper context and would help better characterize native $Ca_v2.1$ channel isoforms.

I also only examined the functional properties of the $Ca_v2.1$ splice variants in co-assembly with the β_4 and $\alpha_2\delta_1$ isoforms of the auxiliary subunits. In native cells, there are multiple isoforms of each auxiliary subunit that can co-assemble with the channels and can potentially cause distinct effects between the splice variants. The heterologous system also lacks other possible $Ca_v2.1$-interacting proteins such as G proteins, γ subunits and synaptic membrane proteins (Zamponi and Snutch, 1998; Rettig *et al.,* 1996; Martin-Moutot *et al.,* 1996; Kim and Catterall 1997; Dolphin, 2012).

Additionally, the electrophysiology experiments were performed in external solution containing barium rather than physiological calcium as the charge carrier thus eliminating the possibility of effects on the calcium-dependent feedback regulation that $Ca_v2.1$ channels undergo via calmodulin binding (Christel and Lee, 2012). Consequently, potential differences between the +SSTR and ΔSSTR $Ca_v2.1$ splice variants towards calcium-dependent facilitation or calcium-dependent inactivation in response to calcium influx are not considered.

5.4 Future directions

An important set of future experiments consist of analyzing and comparing the effects of mutations implicated in FHM1, EA2 and SCA6 disorders on ΔSSTR and +SSTR channel properties to determine whether there are any splice variant-specific differential effects. Diverse effects between the splice variants resulting from mutations could help clarify the localization of pathophysiology of these diseases to specific regions of the CNS. For example, the +SSTR variant is more abundantly expressed in the brainstem and thalamus regions which may be

involved in FHM1 pathophysiology (Pietrobon, 2010; Park *et al.*, 2014). Therefore, it would be of great interest to see whether the +SSTR variant has more pronounced gain-of-function effects generally seen with FHM1 mutations than the ΔSSTR variant (Pietrobon, 2010). Additionally, one EA2 mutation also causes absence epilepsy symptoms which could be a result of it imparting more pronounced effects on +SSTR channels which are expressed in high abundance in the reticular thalamus (Imbrici *et al.*, 2004). In support of this hypothesis, the thalamus of genetic absence epilepsy rats from Strasbourg (GAERS), in comparison to nonepileptic control rats, expresses a greater abundance of a $Ca_v3.2$ channel splice variant that exhibits significant gain-of-function effects due to an absence epilepsy mutation (Powell *et al.*, 2009). Lastly, if the +SSTR and –NP variants do in fact have similar contextual expression patterns due to common regulatory splicing factors, +SSTR may also have an influence on the Purkinje-specific cell loss seen in SCA6 as Purkinje cells predominantly express the –NP variant.

Splice variant-specific effects due to $Ca_v2.1$ mutations allows for the possibility of targeting only dysfunctional $Ca_v2.1$ channels with therapeutic methods while leaving normal functioning channels unaffected and thus preventing harmful off-target side effects. In fact, the specificity of polyQ expansions that underlie SCA6 pathophysiology for the +47 variant of $Ca_v2.1$ inspired one group to develop splice variant-specific RNAi that specifically target the +47 splice variant (Tsou *et al.*, 2011). Impressively, this method managed to suppress polyQ-containing $Ca_v2.1$ channels selectively.

Another therapeutic avenue is through the development of drugs that are based on the structural properties of naturally occurring peptide toxins. As my findings show that the +SSTR variant does not alter the sensitivity of $Ca_v2.1$ to ω-Aga-IVA, +SSTR variant $Ca_v2.1$ channels are eligible targets for potential ω-Aga-IVA mimetics that could treat hyperactive cells or tissues in

$Ca_v2.1$ channelopathies (McDonough, 2007; Nimmrich and Gross, 2012). This method is currently being developed for $Ca_v2.2$ N-type channels which are implicated in chronic pain (Swayne and Bourinet, 2008). Mimetics of ω-conotoxin-GVIA, a highly selective $Ca_v2.2$ channel blocker, are being developed by adjusting physiochemical properties in order increase effectiveness via lowering the molecular weight and binding affinity (Tranberg *et al.,* 2012; Gleeson *et al.,* 2015).

A recent study has also shown that the synthetic phenolic compound 2,5'-di(tertbutyl)-1,4,-benzohydroquinone (BHQ) can "correct" the gating and synaptic transmission defects caused by a severe FHM1 mutation in $Ca_v2.1$ channels by altering channel properties (Inagaki *et al.,* 2014). BHQ inhibits the voltage-dependence of activation, slows deactivation and potentiates CDF in order to offset the harmful gain-of-function effects of the FHM1 mutation. The binding location and potential splice variant-specific effects of BHQ have not yet been determined.

5.5 Conclusions

VGCCs represent a major mechanism by which cells mediate the levels of calcium ions essential for many different physiological processes. Although basic diversity of VGCC functions are provided by the ten different genes encoding the α_1 subunits, further complexity is achieved through alternative splicing in key domains. This leads to a greater diversity in channel properties and subsequently channel activity that is thought to refine calcium entry and regulate VGCC-mediated processes. Here, I have shown the differential expression of the $Ca_v2.1$ channel +SSTR and ΔSSTR splice variants in the rat CNS suggesting that the variants play distinct roles spatially in the CNS and may influence the localized pathophysiology of $Ca_v2.1$-implicated disorders. Further, I have described the effects of the SSTR insertion on the biophysical

properties of $Ca_v2.1$ channels which in at least one instance translate into distinct responses between the +SSTR and ΔSSTR variants to different APWs. As such, the different splice variants likely mediate specific roles essential to CNS synaptic physiology. Lastly, I have shown that the SSTR insertion does not affect the sensitivity of $Ca_v2.1$ channels to ω-Aga-IVA indicating that SSTR-containing $Ca_v2.1$ isoforms are suitable targets for the development of therapeutic drugs that are based on ω-Aga-IVA properties.

References

Adams ME. (2004) Agatoxins: ion channel specific toxins from the american funnel web spider, *Agelenopsis aperta.* Toxicon. 43: 509-525.

Adams PJ, Garcia E, David LS, Mulatz KJ, Spacey SD, and Snutch TP. (2009). Cav2.1 P/Q-type calcium channel alternative splicing affects the functional impact of familial hemilegic migraine mutations. Channels 3(2): 110-121.

Allen SE, Darnell RB and Lipscombe D. (2010). The neuronal splicing factor Nova controls alternative splicing in N-type and P-type Ca_v2 calcium channels. Channels 4(6): 483-489.

Armstrong CM and Matteson DR. (1985). Two distinct populations of calcium channels in a clonal line of pituitary cells. Science 227(4682): 65-67.

Bean BP. (2007). The action potential in mammalian central neurons. Nature Reviews Neuroscience 8: 451-465.

Bezanilla F. (2000). The Voltage Sensor in Voltage-Dependent Ion Channels. Physiological Reviews 80(2): 555-592.

Bezanilla F. (2002). Voltage Sensor Movements. J. Gen. Physiol. 120: 465-473.

Bezprozvanny I, Scheller RH and Tsien RW. (1995). Functional impact of syntaxin on gating of N-type and Q-type calcium channels. Nature 378: 623-626.

Black DL. (2003). Mechanisms of Alternative Pre-Messenger RNA Splicing. Annu. Rev. Biochem. 72: 291-336.

Bolay H, Reuter U, Dunn AK, Huang Z, Boas DA and Moskowitz MA. (2002). Intrinsic brain activity triggers trigeminal meningeal afferents in a migraine model. Nature Medicine 8(2): 136-142.

Borst JGG and Sakmann B. (1999). Effect of changes in action potential shape on calcium currents and transmitter release in a calyx-type synapse of the rat auditory brainstem. Phil. Trans. R. Soc. Lond. B 354: 347-355.

Bourinet E, Soong TW, Sutton K, Slaymaker S, Mathews E, Monteil A, Zamponi GW, Nargeot J and Snutch TP. (1999). Splicing of α_{1A} subunit gene generates phenotypic variants of P- and Q-type calcium channels. Nature neuroscience 2(5): 407-415.

Brody DL, Patil PG, Mulle JG, Snutch TP and Yue DT. (1997). Bursts of action potential waveforms relieve G-protein inhibition of recombinant P/Q-type Ca^{2+} channels in HEK 293 cells. Journal of Physiology 499(3): 637-644.

Catterall WA. (2000). Structure and Regulation of Voltage-Gated Ca2+ Channels. Annu. Rev. Cell Dev. Biol. 16: 521-555.

Catterall WA. (2010). Ion channel voltage sensors: structure, function, and pathophysiology. Neuron 67(6): 915-928.

Catterall WA, Cestele S, Yarov-Yarovoy V, Yu FH, Konoki K and Scheuer T. (2007). Voltage-gated ion channels and gating modifier toxins. Toxicon 49: 124-141.

Catterall WA, Dib-Hajj S, Meisler MH and Pietrobon D. (2008). Inherited Neuronal Ion Channelopathies: New Windows on Complex Neurological Diseases. The Journal of Neuroscience 28(46): 11768-11777.

Catterall WA, Perez-Reyes E, Snutch TP and Striessnig J. (2005). International Union of Pharmacology. XLVIII. Nomenclature and Structure-Function Relationships of Voltage-Gated Calcium Channels. Pharmacol Rev 57: 411-425.

Chang SY, Yong TF, Yu CY, Liang MC, Pletnikova O, Troncoso J, Burgunder JM and Soong TW. (2007). Age and gender-dependent alternative splicing of P/Q-type calcium channel EF-hand. Neuroscience 145: 1026-1036.

Charvin N, Leveque C, Walker D, Berton F, Raymond C, Kataoka M, Shoji-Kasai Y, Takahashi M, De Waard M and Seagar MJ. (1997). Direct interaction of the calcium sensor protein synaptotagmin I with a cytoplasmic domain of the α1A subunit of the P/Q-type calcium channel. The EMBO Journal 16(15): 4591-4596.

Chaudhuri D, Alseikhan BA, Chang SY, Soong TW and Yue DT. (2005). Developmental Activation of Calmodulin-Dependent Facilitation of Cerebellar P-Type Ca^{2+} Current. The Journal of Neuroscience 25(36): 8282-8294.

Chaudhuri D, Chang SY, DeMaria CD, Alvania RS, Soong TW and Yue DT. (2004). Alternative Splicing as a Molecular Switch for $Ca^{2+/}$Calmodulin-Dependent Facilitation of P/Q-Type Ca^{2+} Channels. The Journal of Neuroscience 24(28): 6334-6342.

Chaudhuri D, Issa JB and Yue DT. (2007). Elementary Mechanisms Producing Facilitation of Cav2.1 (P/Q-type) Channels. The Journal of General Physiology 129(5): 385-401.

Christel C and Lee A. (2012). Ca^{2+}-dependent modulation of voltage-gated Ca^{2+} channels. Biochimica et Biophysica Acta 1820: 1243-1252.

Day NC, Wood SJ, Ince PG, Volsen SG, Smith W, Slater CR and Shaw P. (1997). Differential Localization of Voltage-Dependent Calcium Channel α_1 Subunits at the Human and Rat Neuromuscular Junction. The Journal of Neuroscience 17(16): 6226-6235.

Davies A, Kadurin I, Alvarez-Laviada A, Douglas L, Nieto-Rostro M, Bauer CS, Pratt WS and Dolphin AC. (2010). The $\alpha_2\delta$ subunits of voltage-gated calcium channels form GPI-anchored proteins, a posttranslational modification essential for function. Proc Natl Acad Sci 107: 1654-1659.

De Jongh KS, Warner C and Catterall WA. (1990). Subunits of Purified Calcium Channels. α2 and δ are encoded by the same gene. The Journal of Biological Chemistry 265(25): 14738-14741.

De Waard M and Campbell KP. (1995). Subunit regulation of the neuronal α_{1A} Ca^{2+} channel expressed in Xenopus oocytes. Journal of Physiology 485(3): 619-634.

De Waard M, Liu H, Walker D, Scott VES, Gurnett CA and Campbell KP. (1997). Direct binding of G protein complex to voltage-dependent calcium channels. Nature 385: 446-450.

De Waard M, Witcher DR, Pragnell M, Liu H and Campbell KP. (1995). Properties of the α_1-β Anchoring Site in Voltage-dependent Ca^{2+} Channels. The Journal of Biological Chemistry 270(20): 12056-12064.

Dolphin AC. (2012). Calcium channel auxiliary α2δ and β subunits: trafficking and one step beyond. Nat Rev Neurosci 13: 542-555.

Ertel EA, Campbell KP, Harpold MM, Hofmann F, Mori Y, Perez-Reyes E, Schwartz A, Snutch TP, Tanabe T, Birnbaumer L, Tsien RW and Catterall WA. (2000). Nomenclature of Voltage-Gated Calcium Channels. Neuron 25: 533-535.

Frontali M. (2001). Spinocerebellar ataxia type 6: Channelopathy or glutamine repeat disorder? Brain Res Bull 56: 227-231.

Gatchel JR and Zoghbi HY. (2005). Diseases of unstable repeat expansion: Mechanisms and common principles. Nat Rev Genet 6: 743-755.

Gehman LT, Stoilov P, Maguire J, Damianov A, Lin CH, Shiue L, Ares M Jr, Mody I and Black DL. (2011). The splicing regulator Rbfox1 (A2BP1) controls neuronal excitation in the mammalian brain. Nature Genetics 43(7): 706-711.

Geiger JRP and Jonas P. (2000). Dynamic Control of Presynaptic Ca2+ Inflow by Fast-Inactivating K+ Channels in Hippocampal Mossy Fiber Boutons. Neuron 28: 927-939.

Giunti P, Mantuano E, Frontali M and Veneziano L. (2015). Molecular mechanism of Spinocerebellar Ataxia type 6: glutamine repeat disorder, channelopathy and transcriptional dysregulation. The multifaceted aspects of a single mutation. Frontiers in Cellular Neuroscience 9(36):1-5.

Gleeson EC, Graham JE, Spiller S, Vetter I, Lewis RJ, Duggan PJ and Tuck KL. (2015). Inhibition of N-Type Calcium Channels by Fluorophenoxyanilide Derivatives. Mar. Drugs 13: 2030-2045.

Graves TD, Imbrici P, Kors EE, Terwindt GM, Eunson LH, Frants RR, Haan J, Ferrari MD, Goadsby PJ, Hanna MG, van den Maagdenberg AMJM and Kullmann DM. (2008). Premature stop codons in a facilitating EF-hand splice variant of $Ca_v2.1$ cause episodic ataxia type 2. Neurobiology of Disease 32: 10-15.

Hans M, Luvisetto S, Williams ME, Spagnolo M, Urrutia A, Tottene A, Brust PF, Johnson EC, Harpold MM, Stauderman KA and Pietrobon D. (1999a). Functional Consequences of Mutations in the Human α1A Calcium Channel Subunit Linked to Familial Hemiplegic Migraine. The Journal of Neuroscience 19(5): 1610-1619.

Hans M, Urrutia A, Deal C, Brust PF, Stauderman K, Ellis SB, Harpold MM, Johnson EC and Williams ME. (1999b). Structural Elements in Domain IV that Influence Biophysical and Pharmacological Properties of Human α_{1A}-Containing High-Voltage-Activated Calcium Channels. Biophysical Journal 76: 1384-1400.

Herlitze S, Garcia DE, Mackie K, Hille B, Scheuer T and Catterall WA. (1996). Modulation of Ca2+ channels by G-protein subunits. Nature 280: 258-262.

Hillman D, Chen S, Aung TT, Cherksey B, Sugimori M and Llinas RR. (1991). Localization of P-type calcium channels in the central nervous system. Proc. Natl. Acad. Sci. 88:7076-7080.

Hillyard DR, Monje VD, Mintz IM, Bean BP, Nadasdi L, Ramachandran J, Miljanich G, Azimi-Zoonooz A, McIntosh JM, Cruz LJ, Imperial JS and Olivera BM. (1992). A New Conus Peptide Ligand for Mammalian Presynaptic Ca2+ Channels. Neuron 9: 69-77.

Hoppa MB, Lana B, Margas W, Dolphin AC and Ryan TA. (2012). α2δ expression sets presynaptic calcium channel abundance and release probability. Nature 486(7401): 122-125.

Hoskins AA and Moore MJ. (2012). The spliceosome: a flexible, reversible macromolecular machine. Trends in Biochemical Sciences 37(5): 179-188.

Imbrici P, Jaffe SL, Eunson LH, Davies NP, Herd C, Robertson R, Kullmann DM and Hanna MG. (2004). Dysfunction of the brain calcium channel $Ca_v2.1$ in absence epilepsy and episodic ataxia. Brain 127: 2682-2692.

Inagaki A, Frank CA, Usachev YM, Benveniste M and Lee A. (2014). Pharmacological Correction of Gating Defects in the Voltage-Gated $Ca_v2.1$ Ca^{2+} Channel due to a Familial Hemiplegic Migraine Mutation. Neuron 81: 91-102.

Ishikawa K, Fujigasaki H, Saegusa H, Ohwada K, Fujita T, Iwamoto H, Komatsuzaki Y, Toru S, Toriyama H, Watanabe M, Ohkoshi N, Shoji S, Kanazawa I, Tanabe T and Mizusawa H. (1999). Abundant expression and cytoplasmic aggregations of α1A voltage-dependent calcium channel protein associated with neurodegeneration in spinocerebellar ataxia type 6. Human Molecular Genetics 8(7): 1185-1193.

Ishikawa T, Kaneko M, Shin HS and Takahashi T. (2005). Presynaptic N-type and P/Q-type Ca2+ channels mediating synaptic transmission at the calyx of Held of mice. J Physiol 568(1): 199-209.

Jarvis SE and Zamponi GW. (2001). Interactions between presynaptic Ca2+ channels, cytoplasmic messengers and proteins of the synaptic vesicle release complex. Trends in Pharmacological Sciences 22(10): 519-525.

Jeng CJ, Chen YT, Chen YW and Tang CY. (2006). Dominant-negative effects of human P/Q-type Ca2+ channel mutations associated with episodic ataxia type 2. Am J Physiol Cell Physiol 290: C1209-C1220.

Jodice C, Mantuano E, Veneziano L, Trettel F, Sabbadini G, Calandriello L, Francia A, Spadaro M, Pierelli F, Salvi F, Ophoff RA, Frants RR and Frontali M. (1997). Episodic ataxia type 2 (EA2) and spinocerebellar ataxia type 6 (SCA6) due to CAG repeat expansion in the CACNA1A gene on chromosome 19p. Hum Mol Genet. 6(11): 1973-1978.

Kim DK and Catterall WA. (1997). Ca^{2+}-dependent and –independent interactions of the isoforms of the α_{1A} subunit of brain Ca^{2+} channels with presynaptic SNARE proteins. Proc. Natl. Acad. Sci. 94: 14782-14786.

Kordasiewicz HB and Gomez CM. (2007). Molecular Pathogenesis of Spinocerebellar Ataxia Type 6. Neurotherapeutics 4: 285-294.

Krovetz HS, Helton TD, Crews AL and Horne WA. (2000). C-Terminal Alternative Splicing Changes the Gating Properties of a Human Spinal Cord Calcium Channel α1A Subunit. The Journal of Neuroscience 20(20): 7564-7570.

Lauritzen M. (1994). Pathophysiology of the migraine aura. The spreading depression theory. Brain 117(Pt 1): 199-210.

Lee A, Wong ST, Gallagher D, Li B, Storm DR, Scheuer T and Catterall WA. (1999). $Ca^{2+/}$calmodulin binds to and modulates P/Q-type calcium channels. Nature 399: 155-159.

Liao P, Zhang HY and Soong TW. (2009). Alternative splicing of voltage-gated calcium channels: from molecular biology to disease. Eur J Physiol 458: 481-487.

Lipscombe D, Allen SE and Toro CP. (2013). Control of neuronal voltage-gated calcium ion channels from RNA to protein. Trends in Neurosciences 36(10): 598-609.

Lorenzon NM and Beam KG. (2000). Calcium channelopathies. Kidney International 57: 794-802.

Luebke JI, Dunlap K and Turner TJ. (1993). Multiple Calcium Channel Types Control Glutamatergic Synaptic Transmission in the Hippocampus. Neuron 11: 895-902.

Martin-Moutot N, Charvin N, Leveque C, Sato K, Nishiki TI, Kozaki S, Takahashi M and Seagar M. (1996). Interaction of SNARE Complexes with P/Q-type Calcium Channels in Rat Cerebellar Synaptosomes. The Journal of Biological Chemistry 271(12): 6567-6570.

Matsuyama Z, Wakamori M, Mori Y, Kawakami H, Nakamura S and Imoto K. (1999). Direct Alteration of the P/Q-Type Ca2+ Channel Property by Polyglutamine Expansion in Spinocerebellar Ataxia 6. The Journal of Neuroscience 19(RC14): 1-5.

McCobb DP and Beam KG. (1991). Action Potential Waveform Voltage-Clamp Commands Reveal Striking Differences in Calcium Entry via Low and High Voltage-Activated Calcium Channels. Neuron 7: 119-127.
McDonough SI. (2007). Gating modifier toxins of voltage-gated calcium channels. Toxicon 49: 202-212.
McDonough SI, Lampe RA, Keith RA, and Bean BP. (1997a). Voltage-dependent inhibition of N- and P-type calcium channels by the peptide toxin ω-grammotoxin-SIA. Mol. Pharmacol 52: 1095-1104.
McDonough SI, Mintz IM and Bean BP. (1997b). Alteration of P-Type Calcium Channel Gating by the Spider Toxin ω-Aga-IVA. Biophysical Journal 72: 2117-2128.
Mintz IM, Adams ME and Bean BP. (1992a). P-Type Calcium Channels in Rat Central and Peripheral Neurons. Neuron 9:85-95.
Mintz IM, Sabatini BL and Regehr WG. (1995). Calcium Control of Transmitter Release at a Cerebellar Synapse. Neuron 15: 675-688.
Mintz IM, Venema VJ, Swiderek KM, Lee TD, Bean BP and Adams ME. (1992b). P-type calcium channels blocked by the spider toxin ω-Aga-IVA. Nature 355: 827-829.
Mochida S, Westenbroek RE, Yokoyama CT, Zhong H, Myers SJ, Scheuer T, Itoh K and Catterall WA. (2003). Requirement for the synaptic protein interaction site for reconstitution of synaptic transmission by P/Q-type calcium channels. PNAS 100(5): 2819-2824.
Mori Y, Friedrich T, Kim MS, Mikami A, Nakai J, Ruth P, Bosse E, Hofmann F, Flockerzi V, Furuichi T, Mikoshiba K, Imoto K, Tanabe T and Numa S. (1991). Primary structure and functional expression from complementary DNA of a brain calcium channel. Nature 350: 398-402.
Moskowitz MA, Bolay H and Dalkara T. (2004). Deciphering Migraine Mechanisms: Clues from Familial Hemiplegic Migraine Genotypes. Annals of Neurology 55(2): 276-280.
Ophoff RA, Terwindt GM, Vergouwe MN, van Eijk R, Oefner PJ, Hoffman SMG, Lamerdin JE, Mohrenweiser HW, Bulman DE, Ferrari M, Haan J, Lindhout D, van Ommen GJ, Hofker MH, Ferrari MD and Frants RR. (1996). Familial Hemiplegic Migraine and Episodic Ataxia Type-2 Are Caused by Mutations in the Ca2+ Channel Gene CACNL1A4. Cell 87: 543-552.
Park J, Moon H, Akerman S, Holland PR, Lasalandra MP, Andreou AP, Ferrari MD, van den Maagdenberg AM and Goadsby PJ. (2014). Differential trigeminovascular nociceptive responses in the thalamus in the familial hemiplegic migraine 1 knock-in mouse: a Fos protein study. Neurobiol Dis 64: 1-7.
Pietrobon D. (2010). $Ca_v2.1$ channelopathies. Eur J Physiol 460: 375-393.
Pietrobon D. (2013). Calcium channels and migraine. Biochimica et Biophysica Acta 1828: 1655-1665.
Pinto A, Iwasa K, Newland C, Newsom-Davis J and Lang B. (2002). The Action of Lambert-Eaton Myasthenic Syndrome Immunoglobulin G on Cloned Human Voltage-Gated Calcium Channels. Muscle & Nerve 25: 715-724.
Powell KL, Cain SM, Ng C, Sirdesai S, David LS, Kyi M, Garcia E, Tyson J, Reid CA, Bahlo M, Foote SJ, Snutch TP and O'Brien TJ. (2009). A Cav3.2 T-type calcium channel point mutation has splice-variant-specific effects on function and segregates with seizure expression in a polygenic rat model of absence epilepsy. J Neurosci 29(2): 371-380.

Pragnell M, De Waard M, Mori Y, Tanabe T, Snutch TP and Campbell KP. (1994). Calcium channel β-subunit binds to a conserved motif in the I-II cytoplasmic linker of the α_1-subunit. Nature 368: 67-70.

Rajapaksha WRAKJS, Wang D, Davies JN, Chen L, Zamponi GW and Fisher TE. (2008). Novel Splice Variants of Rat Cav2.1 That Lack Much of the Synaptic Protein Interaction Site Are Expressed in Neuroendocrine Cells. The Journal of Biological Chemistry 283(23): 15997-16003.

Randall A and Tsien RW. (1995). Pharmacological Dissection of Multiple Types of Ca2+ Channel Currents in Rat Cerebellar Granule Neurons. The Journal of Neuroscience 15(4): 2995-3012.

Regehr WG and Mintz IM. (1994). Participation of Multiple Calcium Channel Types in Transmission at Single Climbing Fiber to Purkinje Cell Synapses. Neuron 12: 605-613.

Rettig J, Sheng ZH, Kim DK, Hodson CD, Snutch TP and Catterall WA. (1996). Isoform-specific interaction of the α_{1A} subunits of brain Ca^{2+} channels with the presynaptic proteins syntaxin and SNAP-25. Proc. Natl. Acad. Sci. 93: 7363-7368.

Rose SJ, Kriener LH, Heinzer AK, Fan X, Raike RS, van den Maagdenberg AMJM and Hess EJ. (2014). The first knockin mouse model of episodic ataxia type 2. Experimental Neurology 261: 553-562.

Saegusa H, Wakamori M, Matsuda Y, Wang J, Mori Y, Zong S and Tanabe T. (2007). Properties of human $Ca_v2.1$ channel with a spinocerebellar ataxia type 6 mutation expressed in Purkinje cells. Mol. Cell. Neurosci. 34: 261-270.

Simms BA and Zamponi GW. (2014). Neuronal Voltage-Gated Calcium Channels: Structure, Function, and Dysfunction. Neuron 82: 24-45.

Soong TW, DeMaria CD, Alvania RS, Zweifel LS, Liang MC, Mittman S, Agnew WS and Yue DT. (2002). Systemic Identification of Splice Variants in Human P/Q-Type Channel $\alpha_1$2.1 Subunits: Implications for Current Density and Ca^{2+}-Dependent Inactivation. The Journal of Neuroscience 22(23):10142-10152.

Spacey SD, Hildebrand ME, Materek LA, Bird TD and Snutch TP. (2004). Functional Implications of a Novel EA2 Mutation in the P/Q-Type Calcium Channel. Ann Neurol 56: 213-220.

Starr TVB, Prystay W and Snutch TP. (1991). Primary structure of a calcium channel that is highly expressed in the rat cerebellum. Proc. Natl. Acad. Sci. 88: 5621-5625.

Stea A, Tomlinson WJ, Soong TW, Bourinet E, Dubel SJ, Vincent SR and Snutch TP. (1994). Localization and functional properties of a rat brain α1A calcium channel reflect similarities to neuronal Q- and P-type channels. Proc. Natl. Acad. Sci. 91: 10576-10580.

Suh BC, Leal K and Hille B. (2010). Modulation of High-Voltage Activated Ca^{2+} Channels by Membrane Phosphatidylinositol 4,5-Bisphosphate. Neuron 67: 224-238.

Sutton KG, McRory JE, Guthrie H, Murphy TH and Snutch TP. (1999). P/Q-type calcium channels mediate the activity-dependent feedback of syntaxin-1A. Nature 401: 800-804.

Swayne LA and Bourinet E. (2008). Voltage-gated calcium channels in chronic pain: emerging role of alternative splicing. Pflugers Arch 456(3): 459-466.

Takahashi T and Momiyama A. (1993). Different types of calcium channels mediate central synaptic transmission. Nature 366: 156-158.

Tang ZZ, Sharma S, Zheng S, Chawla G, Nikolic J and Black DL. (2011). Regulation of the Mutually Exclusive Exons 8a and 8 in the CaV1.2 Calcium Channel Transcript by Polypyrimidine Tract-binding Protein. The Journal of Biological Chemistry 286(12): 10007-10016.

Tang ZZ, Zheng S, Nikolic J and Black DL. (2009). Developmental Control of CaV1.2 L-Type Calcium Channel Splicing by Fox Proteins. Molecular and Cellular Biology 29(17): 4757-4765.

Toru S, Murakoshi T, Ishikawa K, Saegusa H, Fujigasaki H, Uchihara T, Nagayama S, Osanai M, Mizusawa H and Tanabe T. (2000). Spinocerebellar Ataxia Type 6 Mutation Alters P-type Calcium Channel Function. J. Biol. Chem. 275: 10893-10898.

Tottene A, Fellin T, Pagnutti S, Luvisetto S, Striessnig J, Fletcher C and Pietrobon D. (2002). Familial hemiplegic migraine mutations increase Ca^{2+} influx through single human $Ca_v2.1$ channels and decrease maximal $Ca_v2.1$ current density in neurons. PNAS 99: 13284-13289.

Tottene A, Pivotto F, Fellin T, Cesetti T, van den Maagdenberg AMJM and Pietrobon D. (2005). Specific Kinetic Alterations of Human $Ca_v2.1$ Calcium Channels Produced by Mutation S218L Causing Familial Hemiplegic Migraine and Delayed Cerebral Edema and Coma after Minor Head Trauma. The Journal of Biological Chemistry 280(18): 17678-17686.

Tranberg CE, Yang A, Vetter I, McArthur JR, Baell JB, Lewis RJ, Tuck KL and Duggan PJ. (2012). ω-Conotoxin GVIA Mimetics that Bind and Inhibit Neuronal $Ca_v2.2$ Ion Channels. Mar. Drugs 10(10): 2349-2368.

Tsou WL, Soong BW, Paulson HL and Rodriguez-Lebron E. (2011). Splice isoform-specific suppression of the $Ca_v2.1$ variant underlying Spinocerebellar ataxia type 6. Neurobiol Dis. 43(3): 533-542.

Tsunemi T, Ishikawa K, Jin H and Mizusawa H. (2008). Cell-type-specific alternative splicing in spinocerebellar ataxia type 6. Neuroscience Letters 447:78-81.

Turner TJ, Adams ME and Dunlap K. (1993). Multiple Ca^{2+} channel types coexist to regulate synaptosomal neurotransmitter release. Proc. Natl. Acad. Sci. 90: 9518-9522.

Uchitel OD, Protti DA, Sanchez V, Cherksey BD, Sugimori M and Llinas R. (1992). P-type voltage-dependent calcium channel mediates presynaptic calcium influx and transmitter release in mammalian synapses. Proc. Natl. Acad. Sci. 89: 3330-3333.

Ule J, Stefani G, Mele A, Ruggiu M, Wang X, Taneri B, Gaasterland T, Blencowe BJ and Darnell RB. (2006). An RNA map predicting Nova-dependent splicing regulation. Nature 444: 580-586.

Usowicz MM, Sugimori M, Cherksey B and Llinas R. (1992). P-type Calcium Channels in the Somata and Dendrites of Adult Cerebellar Purkinje Cells. Neuron 9:1185-1199.

Wan J, Khanna R, Sandusky M, Papazian DM Jen JC and Baloh RW. (2005). CACNA1A mutations causing episodic and progressive ataxia alter channel trafficking and kinetics. Neurology 64(12): 2090-2097.

Wappl E, Koschak A, Poteser M, Sinnegger MJ, Walter D, Eberhart A, Groschner K, Glossmann H, Kraus RL, Grabner M and Striessnig. (2002). Functional Consequences of P/Q-type Ca2+ Channel Cav2.1 Missense Mutations Associated with Episodic Ataxia Type 2 and Progressive Ataxia. The Journal of Biological Chemistry 277(9): 6960-6966.

Watase K, Barrett CF, Miyazaki T, Ishiguro T, Ishikawa K, Hu Y, Unno T, Sun Y, Kasai S, Watanabe M, Gomez CM, Mizusawa H, Tsien RW and Zoghbi HY. (2008). Spinocerebellar ataxia type 6 knockin mice develop a progressive neuronal dysfunction with age-dependent accumulation of mutant $Ca_v2.1$ channels. PNAS 105(33): 11987-11992.

Westenbroek RE, Hoskins L and Catterall WA. (1998). Localization of Ca2+ Channel Subtypes on Rat Spinal Motor Neurons, Interneurons, and Nerve Terminals. The Journal of Neuroscience 18(16): 6319-6330.

Westenbroek RE, Sakurai R, Elliot EM, Hell JW, Starr TVB, Snutch TP and Catterall WA. (1995). Immunochemical Identification and Subcellular Distribution of the α_{1A} Subunits of Brain Calcium Channels. The Journal of Neuroscience 15(10): 6403-6418.

Wheeler DB, Randall A and Tsien RW. (1994). Roles of N-type and Q-type Ca2+ channels in supporting hippocampal synaptic transmission. Science 264(5155): 107-111.

Winterfield JR and Swartz KJ. (2000). A Hot Spot for the Interaction of Gating Modifier Toxins with Voltage-dependent Ion Channels. J. Gen. Physiol. 116: 637-644.

Wu L, Bauer CS, Zhen XG, Xie C and Yang J. (2002). Dual regulation of voltage-gated calcium channels by PtdIns(4,5)P_2. Nature 419(6910): 947-952.

Yang YYL, Yin GL and Darnell RB. (1998). The neuronal RNA-binding protein Nova-2 is implicated as the autoantigen targeted in POMA patients with dementia. Proc. Natl. Acad. Sci. 95: 13254-13259.

Zamponi GW and Snutch TP. (1998). Modulation of voltage-dependent calcium channels by G proteins. Current Opinion in Neurobiology 8: 351-356.

Zhong H, Yokoyama CT, Scheuer T and Catterall WA. (1999). Reciprocal regulation of P/Q-type Ca2+ channels by SNAP-25, syntaxin and synaptotagmin. Nature Neuroscience 2(11): 939-941.

Zhuchenko O, Bailey J, Bonnen P, Ashizawa T, Stockton DW, Amos C, Dobyns WB, Subramony SH, Zoghbi HY, and Lee CC. (1997). Autosomal dominant cerebellar ataxia (SCA6) associated with small polyglutamine expansions in the α_{1A}-voltage-dependent calcium channel. Nature genetics 15: 62-69.